Copy 227
RM A54E12

NACA RM A54E12

NACA

RESEARCH MEMORANDUM

A FLIGHT INVESTIGATION AT TRANSONIC SPEEDS OF THE AERODYNAMIC CHARACTERISTICS OF A MODEL HAVING A THIN UNSWEPT WING OF ASPECT RATIO 3.1

By Maurice D. White

Ames Aeronautical Laboratory
Moffett Field, Calif.

NATIONAL ADVISORY COMMITTEE
FOR AERONAUTICS

WASHINGTON

August 4, 1954

NATIONAL ADVISORY COMMITTEE FOR AERONAUTICS

RESEARCH MEMORANDUM

A FLIGHT INVESTIGATION AT TRANSONIC SPEEDS OF THE AERODYNAMIC CHARACTERISTICS OF A MODEL HAVING A THIN UNSWEPT WING OF ASPECT RATIO 3.1

By Maurice D. White

SUMMARY

Free-falling recoverable-model tests have been conducted at transonic speeds on a model having a low-aspect-ratio thin unswept wing and a 45° swept tail located in the chord plane of the wing. Static- and dynamic-stability data and load-distribution data were obtained at angles of attack up to about 12° to 20° depending on the Mach number. The most significant variations noted in the results were those due to nonlinearities with angle of attack of both the wing and the tail characteristics. Over the test range of angles of attack and Mach numbers, the aerodynamic center moved one half of the mean aerodynamic chord partly because both wing and tail contributed less stability at low angles of attack than at high angles of attack. The tail effectiveness was reduced at low angles of attack, and the flight-determined values of the damping-in-pitch parameter showed considerable scatter, presumably as a result of nonlinear variation with angle of attack of the dynamic pressure and downwash at the tail. No buffeting was experienced, however, except in regions of high-lift stall.

INTRODUCTION

As part of a general investigation of the characteristics of various low-aspect-ratio wings, flight tests were conducted on a model having a thin straight wing of aspect ratio 3.1. Wind-tunnel tests reported in references 1 and 2 presented the static longitudinal characteristics, at subsonic and supersonic speeds, of two configurations having wings of the same plan form as the wing of the present tests. In the present tests the range of the wind-tunnel investigation was extended in the following particulars:

1. Transonic Mach numbers were covered - the Mach numbers ranged from 0.80 to 1.16.

2. The tests were made at higher Reynolds numbers - Reynolds numbers ranged from 6-1/2 million to 12-1/2 million.

3. Aerodynamic characteristics were obtained for the complete model (wing-body-tail) as well as for the wing alone.

4. Dynamic- as well as static-stability characteristics of the model were obtained.

5. Loading distributions over the model were obtained.

The tests were made by the Ames Laboratory using the free-falling recoverable-model technique in an area provided by the Air Force at Edwards Air Force Base, Muroc, California.

SYMBOLS

b	wing span, ft
c	local chord, ft
$\bar{c}$	mean aerodynamic chord of the wing, $\frac{2}{S}\int_0^{b/2} c^2 dy$, ft
I_y	moment of inertia of the model about the Y axis, slug-ft^2
M	Mach number
m	twisting couple applied at wing tip, ft-lb
p	static pressure at a fuselage orifice, lb/sq ft
ΔP	$\frac{p_l - p_u}{q_o}$
q_o	dynamic pressure, lb/sq ft
$\dot{q}$	angular acceleration in pitch, radians/sec^2
r	radius of fuselage at longitudinal station x, in.
S	wing area, including portion of wing covered by fuselage, sq ft
x	longitudinal distance from fuselage station 0, in.
y	spanwise distance from model center line, ft

V	speed, ft/sec
$\frac{t}{c}$	ratio of maximum thickness to the chord of the wing
C_D	drag coefficient, $\frac{\text{drag}}{q_o S}$
C_L	lift coefficient, $\frac{\text{lift}}{q_o S}$
C_m	pitching-moment coefficient, $\frac{\text{pitching moment}}{q_o S \bar{c}}$
C_n	yawing-moment coefficient, $\frac{\text{yawing moment}}{q_o S b}$
α	angle of attack, deg
β	angle of sideslip, deg
δ	deflection of horizontal tail, deg
ϵ	downwash angle, deg
θ	angle of twist, deg

Subscripts

e	exposed wing panels
l	lower
q	rate of pitch, $\frac{q\bar{c}}{2V}$
T	complete model
t	horizontal tail
u	upper
w	total wing
max	maximum
min	minimum

$\dot{\alpha}$ rate of change of angle of attack, $\frac{\dot{\alpha}\bar{c}}{2V}$

α,β,δ derivative of the factor with respect to the subscript, as $C_{L_\alpha} = \frac{\partial C_L}{\partial \alpha}$, etc.

MODEL

A three-view drawing of the complete model is shown in figure 1 and additional pertinent dimensions are listed in table I. A photograph of the model, taken immediately after release from the carrier airplane, is shown in figure 2. Shown attached to the model in figure 2 is the booster which was used in some of the tests to obtain higher Mach numbers.

The wing of the model was of the same plan form as that of the wings of references 1 and 2. The airfoil section of the wing was the same as that of the wing of reference 2; that is, semielliptical from 0 to 50 percent of the chord, and biconvex from 50 to 100 percent of the chord (table II). The wing panels were constructed of solid aluminum alloy, and the juncture of the wing root and the fuselage was sealed with a flexible rubber seal.

All other components of the model were as described in reference 3.

INSTRUMENTATION

The following quantities were recorded continuously on two oscillographs:

Quantity	Transducer
Angles of attack and sideslip	Selsyns geared to vanes mounted on boom ahead of body (fig. 1)
Rates of pitch and roll	Doelcam gyroscopes
Angular acceleration in pitch	Statham angular accelerometer
Vertical and longitudinal acceleration	Statham linear accelerometers
Wing balance loads	Strain gages (See ref. 3 for details)

The following quantities were obtained from records on NACA continuously recording instruments:

Quantity	Instrument
Horizontal- and vertical-tail deflections	NACA 2-component control position recorder
Mach number and dynamic pressure	NACA 6-cell manometer
Differential pressure between orifices on upper and lower surfaces of fuselage	NACA 6-cell manometers
Deflection of wing tip	16 mm GSAP movie camera mounted in fuselage and sighting along wing span

All the flight records were synchronized by a chronometric timer. The airspeed system was calibrated at different angles of attack using the SCR584 radar installation of the NACA High-Speed Flight-Research Station at Edwards Air Force Base.

TESTS

The test procedure used was the same as that described in reference 3; that is, after attaining the test Mach number, the horizontal control was pulsed intermittently, and data were recorded during the ensuing oscillations. For some drops rocket assist was employed in order to increase the attainable Mach number. The booster rocket (fig. 2) was jettisoned at the conclusion of boost and prior to the actual test period.

The results presented herein were obtained in four drops and cover a Mach number range from 0.80 to 1.16, a Reynolds number range from 6-1/2 million to 12-1/2 million (fig. 3), and angles of attack from -4° to about 20° for Mach numbers less than 0.9, and angles of attack from -4° to about 12° for Mach numbers greater than 0.9.

Supplementary ground tests were also made to determine the deflection characteristics of the wing. The elastic-axis location and the torsional stiffness of the wing were determined by applying a twisting couple at the wing tip. A concentrated load was applied successively at several points along the elastic axis to determine the bending curve of the wing.

PRECISION OF MEASUREMENT

The instruments used in the present investigation were of the same accuracy as those used in the investigation of reference 3. It follows then that the error of any single value of the angle of attack or Mach number is equal to the values given in reference 3, and the error of any

single value of an aerodynamic coefficient is reduced by the ratio of the appropriate wing dimensions. Application of these factors leads to the following values:

Item	Estimated maximum error M = 0.85	M = 1.05
C_{L_T}	±0.01	±0.004
C_{L_e} and C_{L_w}	±.01	±.003
C_{D_T}	±.001	±.001
C_{D_e} and C_{D_w}	±.003	±.001
C_{m_T}	±.002	±.001
C_{m_e} and C_{m_w}	±.001	±.001
Mach number	±.01	±.01
Angle of attack	±1/4°	±1/4°

The over-all accuracy of the final results is, of course, a function of factors additional to the precision of the instruments, but to which it is difficult to assign quantitative values. For example, the accuracy of any one "static" data point is reduced by the fact that it is determined through time correlation of a number of rapidly varying records. However, in deriving the curves showing the variation of a "static" quantity with, say, angle of attack, a large volume of data points is considered, which helps to define more closely the correct fairing of the data. Also, shifts in the data which occurred from drop to drop were usually definable to a close degree by reference to a number of different records, and by the fact that the entire configuration was symmetrical with control undeflected. Consideration of all these factors leads to the conclusion that the accuracy of "static" results which were obtained by fairing the flight data is of the order of the values listed above.

RESULTS

In general, the flight data were evaluated by the methods described in reference 3. The results are identified as applying to the following:

1. The exposed wing panels.
2. The total wing, obtained by adding to the data for the exposed wing panels, the data obtained by integrating the pressure differences over the fuselage between stations 60 and 135. An additional total-wing drag increment was obtained by applying a skin-friction coefficient of 0.0028 to the entire fuselage surface area between stations 60 and 135.
3. The total model.

Lift

In figure 4 curves are presented of C_L against α for the test Mach number range, and in figure 5 the lift-curve slopes for the various components are plotted as a function of Mach number. In presenting the lift-curve slopes for the complete model in figure 5, it was assumed that the slopes were unaffected by deflections of the horizontal tail. Values of $C_{L_{max}}$ and α for $C_{L_{max}}$ for the various components are plotted as a function of Mach number in figure 6; these values are available only for Mach numbers less than 0.92 because of the limited range of angles of attack covered at high Mach numbers.

Drag

Curves of C_D against C_L for the various components are plotted in figure 7 for various Mach numbers. In figures 8(a), 8(b), and 8(c) are plotted, respectively, as a function of Mach number, the values of $C_{D_{min}}$ for the total wing and for the total model, the values of the drag-rise factor $\partial C_D/\partial C_L{}^2$ for the total wing, and the values of $\partial C_D/\partial C_L{}^2$ for the total model.

Static Longitudinal Stability

The variation with Mach number of trim angle of attack for each of several horizontal-tail positions is shown in figure 9.

In figures 10(a) and 10(b) are shown the variation with angle of attack of C_{m_T} and C_{m_e} for several Mach numbers. The values of C_{m_T} were determined from the expression $C_{m_T} = I_y\dot{q}/q_oS\bar{c}$. Also shown in figure 10(a) are straight lines having the slope $C_{m_{\alpha_T}}$ as determined from the periods of the oscillations that occurred about $\alpha = 0^\circ$. For clarity, the lines are drawn displaced in C_m from their actual locations, but each line is limited to the angle-of-attack range covered by the particular half-cycle of data used. The lines drawn from $\alpha = 0^\circ$ to α_{max} or to α_{min} represent values obtained from the rate-of-pitch records for each cycle, while lines drawn from α_{min} to α_{max} represent values obtained from the angle-of-attack records for each cycle.

Curves of C_{m_T} against α have been calculated for $\delta = 0^\circ$ for the complete angle-of-attack ranges covered by the tests by applying corrections to the data of figure 10(a) for differences in center-of-gravity location and in horizontal-tail setting. These calculated curves

are presented in figure 11 together with corresponding curves for the exposed wing panels and the total wing. The pitching-moment coefficients for the tail with $\delta = 0^\circ$, as determined by subtracting from the total model data the data for the total wing, are also included in figure 11. It will be noted that by this method of evaluation, the value of C_{m_T} will include the contribution to C_m of the portion of the fuselage forward of the region where pressures were measured. The magnitude of this contribution is believed to be inconsequential in relation to that of the tail.

The wing pitching moments about the wing quarter-chord point have been cross-plotted in figure 12 in terms of C_{m_e} against C_{L_e}, and C_{m_w} against C_{L_w}. The variations with Mach number of the aerodynamic-center location for various components of the model are shown in figure 13(a).

The longitudinal-stability data generally indicate differences in stability between what might be called "low" and "high" angle-of-attack ranges. The value of C_L at which the stability changes is shown as a function of Mach number in figure 13(b).

Dynamic Longitudinal Stability

Values of $C_{m_q} + C_{m_{\dot{\alpha}}}$ are shown in figure 14 as a function of Mach number. These values were obtained in the usual manner; that is, by deducting the contribution of the lift-curve slope from the total damping factor that was obtained from analysis of the control-fixed oscillations of the model.

Horizontal-Tail Effectiveness

The variation with Mach number of the horizontal-tail-effectiveness parameter C_{m_δ} is shown in figure 15. Two methods were used to evaluate this parameter. One method was to plot C_{m_T} against δ during a control pulse, selecting data only for regimes where α was reasonably constant. The second method used was to plot as a function of $\Delta\delta_{trim}$ the change in C_{m_T} that would be required to aline the curves of figure 10(a) for $\delta \neq 0^\circ$ with those for $\delta = 0^\circ$ shown in figure 11.

Loading Distribution Over Fuselage

In figure 16 are plotted the distributions of loading along the fuselage center line and along a line displaced 45° from the center line.

The locations of the orifices from which the data were obtained are shown in figure 17. The data represent the difference in pressure coefficient between corresponding orifices on the top and bottom of the fuselage.

Buffet Boundary

The records of all the drops were examined for evidence of buffeting, but no indication of buffeting was apparent except in regions where the wing was stalled at high lift ($C_{L_e} \approx 0.55$).

Directional Stability

Values of the directional-stability parameter C_{n_β} were deduced from the periods of random oscillations that occurred in two drops and are shown in figure 18 as a function of Mach number. The trim angles of attack corresponding to the identifying horizontal-control deflections of 0° and $-11\text{-}1/2^\circ$ are shown in figure 9.

DISCUSSION

Lift

At subsonic Mach numbers the lift curves of figure 4 show definite nonlinearities, the slopes of the curves increasing with increasing angle of attack. Similar trends were shown by the data of reference 2, plotted in figure 4 for comparison at Mach numbers of 0.80 and 0.92.

The lift-curve slopes of the total wing are compared in figure 19 with values obtained for models having similar wings and tested in other facilities, as reported in references 4 and 5. As shown, the present values are somewhat lower than those obtained in the other tests. The aeroelastic characteristics of the wing were considered as a cause of this difference, but ground measurements of the wing twist, described in Appendix A, which were confirmed by flight measurements, indicated this effect to be an insignificant factor. Differences in relative size of wing and fuselage were also examined as a possible cause, but again the effects proved negligible. The cause of the difference is unresolved at this time.

Drag

In figure 8(a) the flight variation of minimum drag coefficient with Mach number is compared with the theoretical variation computed by adding to the subsonic value the increment determined by the method described in reference 6. The computed and flight curves are seen to be in reasonably good agreement with each other.

In figures 8(b) and 8(c) the experimental drag rise with lift, expressed in terms of the factor $\partial C_D/\partial C_L^2$, is compared with values computed assuming (1) an elliptical spanwise distribution of lift at subsonic speeds ($1/\pi A$) and (2) the resultant force vector perpendicular to the wing chord ($1/57.3\ C_{L_\alpha}$). Low-lift values of C_{L_α} were used in the expression $1/57.3\ C_{L_\alpha}$. The results indicate that the resultant force vector is inclined only a small amount from perpendicularity to the wing chord at a Mach number of 0.8; with increasing Mach number, the vector becomes more nearly perpendicular until, at Mach numbers greater than 0.96, it is nearly completely so.

Static Longitudinal Stability

The present results show the aerodynamic-center movement of the complete model to be very large when the entire range of conditions covered in the tests is considered (fig. 13(a)). The aerodynamic center moves from $0.21\bar{c}$ at a Mach number of 0.88 at "low" C_L's to $0.74\bar{c}$ at Mach numbers greater than 1.08 for "high" C_L's, a shift of $0.53\bar{c}$. This large aerodynamic-center movement results from the fact that both the wing and the tail contribute less stability at low angles of attack than at high angles of attack. With high tail positions the reductions in stability contribution of the tail tend to occur at higher angles of attack, rather than at low angles of attack, and this modification would appear a suitable means for decreasing the overlarge aerodynamic-center travel experienced on this model with the tail in the wing chord plane. Reference 7, for example, shows an aerodynamic-center variation of $0.24\bar{c}$ over a comparable range of test conditions for a higher tail location behind a similar wing.

As indicated in figure 11, the contribution of the horizontal tail to the static stability is nearly nil at small angles of attack. The range of angles of attack over which this effect persists is greatest at a Mach number of 0.97, and it diminishes with either increase or decrease of Mach number from this value, being, however, evident to some extent at all test Mach numbers. Tail-effectiveness data (C_{m_δ}) to be discussed later show only a decrease rather than a complete loss in tail effectiveness at small angles of attack as compared with higher angles of attack

(fig. 15). It follows then that the complete loss in tail contribution to stability at small angles of attack must result from a large effective value of $\partial\epsilon/\partial\alpha$, approaching 1.0 in magnitude. Reference 8 shows similar reductions in tail contribution to the stability at small angles of attack for a tail located in the chord plane of a straight wing of aspect ratio 4, for Mach numbers near 0.95, and it is shown there that the increase in $\partial\epsilon/\partial\alpha$ at small angles of attack is the main cause of this effect. It is of interest to note, however, that transonic-bump tests of a similar wing, reported in reference 9, failed to indicate as great a variation of $\partial\epsilon/\partial\alpha$ with angle of attack at these Mach numbers. Some of this increased value of $\partial\epsilon/\partial\alpha$ could be charged to the usual increase in downwash within the wing wake, associated with an increased wake width as the wing drag coefficient becomes greater. However, the diminution of the effect at Mach numbers greater than 0.97 which occurs despite the fact that the drag coefficient is still increasing suggests that other unidentified effects also contribute to maintaining a high effective value of $\partial\epsilon/\partial\alpha$.

The low-angle-of-attack variation with Mach number of the wing aerodynamic-center position is compared in figure 20 with those of several models having similar wings, but of biconvex airfoil section, reported in reference 4. The flight results are seen to be in good agreement with the average of the data from several facilities.

There were insufficient test data from the other facilities to permit similar comparisons at high angles of attack. However, comparisons are made in figure 12 of the variations of the wing pitching-moment coefficient with angle of attack with those reported in reference 2 for several Mach numbers. The results show only minor differences between the flight and the wind-tunnel data, the greatest difference being at a Mach number of 0.80 where the wind-tunnel data show the tendency for a stable break in the curve to occur at a higher value of C_L than do the flight data.

Dynamic Longitudinal Stability

The flight test results in figure 14 show a general tendency toward increasing negative values of $C_{m_q} + C_{m_{\dot{\alpha}}}$ with increasing Mach number, but the scatter of the data precludes the fitting of a curve to the data. It appears that there may be an explanation for this scatter in addition to that of the inherent difficulty of determining values of $C_{m_q} + C_{m_{\dot{\alpha}}}$ accurately from flight data; that is, the values of $C_{m_q} + C_{m_{\dot{\alpha}}}$ may vary with angle of attack. The preceding discussion of static stability noted the evidence of increased values of $\partial\epsilon/\partial\alpha$ and reduced tail effectiveness at small angles of attack as compared with large angles of attack. These two factors are of compensating sign but not necessarily compensating

magnitude as regards their effect on the value of $C_{m_q} + C_{m_{\dot{\alpha}}}$, and it should, therefore, not be surprising to find inconsistencies among values obtained from tests covering different ranges of angles of attack.

The actual variations of model and of wing pitching-moment coefficients with angle of attack obtained in flight are shown in figure 10 in order to illustrate their nature. From the difference in hysteresis-loop widths of the complete model and the wing data, it is apparent that most of the damping is contributed by the tail. Some attempts were made to match the variations of the data for the model on a high-speed electronic simulator, using nonlinear mean variations of C_m with α, and a second-order equation with linear damping. These were helpful in defining the shape of the mean curve of C_m with α, but the matchings of the resultant curves were only moderately good, and it is inferred from this also that the damping would have to be made a function of angle of attack to provide satisfactory matchings of the flight data.

The general level of the flight values of $C_{m_q} + C_{m_{\dot{\alpha}}}$ are in agreement with values estimated as described in reference 10. Approximately five sixths of the estimated values result from the tail. In estimating the tail contribution, tail lift-curve slopes presented in reference 10 were used. Modification of the tail lift-curve slopes to agree with the C_{m_δ} variations of figure 15 would not have improved the over-all agreement of the flight and the estimated values of $C_{m_q} + C_{m_{\dot{\alpha}}}$.

Horizontal-Tail Effectiveness

Horizontal-tail-effectiveness data from the present tests (fig. 15) agree reasonably well with data from reference 10 (appropriately corrected for wing dimensions) which covered tests of the same tail located similarly but behind a wing of different plan form. At Mach numbers less than about 0.92 there are significant differences between the data from the present tests and those from reference 10, which are believed to be associated with the angle-of-attack range represented by the particular data. The pulse data for the present tests are only for low angles of attack for these Mach numbers, and presumably represent conditions where the tail was immersed in the wing wake. The data from reference 10, on the other hand, cover higher angles of attack where the tail would have emerged from the wing wake.

For Mach numbers greater than 1.0 there are indications from the trim data of a substantial reduction in horizontal-tail effectiveness at low angles of attack as compared with higher angles of attack, amounting to about a 33-percent reduction. Since the tail is operating at relatively small angles of attack for the regions of reduced effectiveness, it appears reasonable to charge the reduction to defects in dynamic pressure

in the wing wake, rather than to a loss in tail lift-curve slope. The failure of the pulse data to confirm the differences due to angle of attack shown by the trim data is presently regarded merely as an indication of the poorer accuracy of the pulse determination of C_{m_δ}.

At Mach numbers between 0.92 and 1.0 the variations of horizontal-tail effectiveness with both angle of attack and Mach number are somewhat erratic, which is not unusual for aerodynamic characteristics in this Mach number range.

SUMMARY OF RESULTS

Flight tests at transonic speeds of a free-falling model incorporating a low-aspect-ratio thin straight wing and a 45° swept horizontal tail located in the chord plane of the wing showed the following results:

1. The complete model had a very large variation of aerodynamic-center position over the test range of Mach numbers (M = 0.80 to 1.16) and angles of attack (up to 12° to 20° depending on the Mach number), amounting to about one half of the mean aerodynamic chord. This large aerodynamic-center movement was at least partly due to the fact that both the wing and the tail contributed lower stability at low angles of attack than at high angles of attack.

2. The lift-curve slopes for the total wing were appreciably less than corresponding values obtained for similar wings tested in combination with fuselages in other test facilities, although the variations with Mach number were generally similar.

3. For the wing the variation of drag with lift was such as to indicate that the resultant force vector was perpendicular to the wing chord for Mach numbers greater than 0.96.

4. There was no indication of buffeting throughout the test range of angles of attack and Mach numbers, except where the wing was stalled at high-lift conditions.

5. The horizontal-tail-effectiveness characteristics indicated losses in dynamic pressure of the order of 33 percent in the wing wake at small angles of attack for Mach numbers greater than 1.0.

6. The values of the damping-in-pitch parameter, $C_{m_q} + C_{m_{\dot{\alpha}}}$, were generally consistent with predictions which attributed most of the effect to the tail. Considerable scatter was evident in the data, which is believed to result, in part, from nonlinearities in the tail characteristics with angle of attack.

Ames Aeronautical Laboratory
National Advisory Committee for Aeronautics
Moffett Field, Calif., May 12, 1954.

APPENDIX A

ELASTICITY TESTS OF THE WING

Ground tests were conducted on the test wing in order to determine its elastic characteristics, and the results are shown in figure 21. The wing was supported at the root between 3 percent and 58 percent of the chord in the same manner as in the flight tests. For this support the elastic axis varied from about 27 percent of the chord at the root to 34 percent of the chord at the tip. Additional twisting tests were conducted with the root supported near the trailing edge as well (see sketch in fig. 21) in order to simulate more closely the wing support of an actual airplane. These results showed only a slight rearward shift in elastic-axis location; that is, the axis ran from 37 percent of the chord at the root to 38 percent of the chord at the tip.

The elastic characteristics of the present wing were compared with those of the wing of reference 2 in order to determine whether the difference in lift-curve slopes of the two wings was due to this factor. For the wing of reference 2 it was known only that the wing had been constructed by adding a tin-bismuth alloy, a relatively inelastic material, to the front part of the biconvex steel wing used in the tests of reference 1. For such a construction it is probable that the elastic axis is not far from the 50-percent-chord point along the entire span.

Assuming this location for the elastic axis of the wing of reference 2, using the experimentally determined location for the flight model wing, and allowing for the differences in material of the two wings (aluminum for the flight wing and steel for the wind-tunnel wing), the difference in effective angle of attack due to twisting was computed for the two wings. The computations indicated that the effects of wing twist would be inadequate to account for a significant portion of the difference in lift-curve slope of the two wings.

REFERENCES

1. Reese, David E., and Phelps, E. Ray: Lift, Drag, and Pitching Moment of Low-Aspect-Ratio Wings at Subsonic and Supersonic Speeds - Plane Tapered Wing of Aspect Ratio 3.1 with 3-Percent-Thick, Biconvex Section. NACA RM A50K28, 1951.

2. Heitmeyer, John C.: Lift, Drag, and Pitching Moment of Low-Aspect-Ratio Wings at Subsonic and Supersonic Speeds - Plane Tapered Wing of Aspect Ratio 3.1 with 3-Percent-Thick Rounded-Nose Section. NACA RM A52D23, 1952.

3. Holdaway, George H.: Comparison of the Aerodynamic Characteristics at Transonic Speeds of a Plane Wing and a Cambered and Twisted Wing, Both Having 45° of Sweepback and an Aspect Ratio of 6. NACA RM A53B16, 1953.

4. Hall, Charles F.: Lift, Drag, and Pitching Moment of Low-Aspect-Ratio Wings at Subsonic and Supersonic Speeds. NACA RM A53A30, 1953.

5. Gillis, Clarence L., and Vitale, James A.: Wing-On and Wing-Off Longitudinal Characteristics of an Airplane Configuration Having a Thin Unswept Tapered Wing of Aspect Ratio 3, as Obtained from Rocket-Propelled Models at Mach Numbers from 0.8 to 1.4. NACA RM L50K16, 1951.

6. Holdaway, George H.: Comparison of Theoretical and Experimental Zero-Lift Drag-Rise Characteristics of Wing-Body-Tail Combinations Near the Speed of Sound. NACA RM A53H17, 1953.

7. McFall, John C., Jr., and Hollinger, James A.: Longitudinal Stability, Control Effectiveness, and Drag Characteristics at Transonic Speeds of a Rocket-Propelled Model of an Airplane Configuration having an Unswept Tapered Wing of Aspect Ratio 3 and NACA 65A004.5 Airfoil Sections. NACA RM L52L04, 1953.

8. Johnson, Ben H., Jr., and Rollins, Francis W.: Investigation of a Thin Wing of Aspect Ratio 4 in the Ames 12-Foot Pressure Wind Tunnel. V - Static Longitudinal Stability and Control Throughout The Subsonic Speed Range of a Semispan Model of a Supersonic Airplane. NACA RM A9I01, 1949.

9. Goodson, Kenneth W., and Morrison, William D., Jr.: Aerodynamic Characteristics of a Wing with Unswept Quarter-Chord Line, Aspect Ratio 4, Taper Ratio 0.6, and NACA 65A006 Airfoil Section. Transonic-Bump Method. NACA RM L9H22, 1949.

10. White, Maurice D.: Effect of Camber and Twist on the Stability Characteristics of Models Having a 45° Swept Wing as Determined by the Free-Fall Method at Transonic Speeds. NACA RM A52F16, 1952.

TABLE I.- DIMENSIONS OF FREE-FALL MODEL

Gross weight, lb	1720 to 1840
Moment of inertia about Y axis, slug-ft^2	954 to 974
Center of gravity	0.055$\bar{c}$ and 0.191$\bar{c}$
Wing	
Area, sq ft	21.7
Area, exposed panels, sq ft	16.6
Aspect ratio	3.1
Taper ratio	0.39
Span, ft	8.19
Mean aerodynamic chord, ft	2.81
Airfoil section	0 to 0.5c Ellipse 0.5 to 1.0c Biconvex t/c = 0.03
Horizontal tail (all-movable, pivoting about axis perpendicular to longitudinal axis of model)	
Area (including 2.0 sq ft included in fuselage)	6.0
Aspect ratio	4.5
Taper ratio	0.20
Span, ft	5.21
Mean aerodynamic chord (including area included in fuselage) ft	1.36
Leading edge of mean aerodynamic chord	Station 153.6
Root chord, ft	1.96
Tip chord, ft	0.40
Airfoil section, parallel to stream	NACA 65006
Gap between tail and fuselage at 0° deflection, in.	1/16
Vertical tail (all-movable differentially, pivoting about axis perpendicular to longitudinal axis of model)	
Area (including 1.4 sq ft included in fuselage), sq ft	3.3
Aspect ratio	5.1
Taper ratio	0.22
Span, ft	4.1
Mean aerodynamic chord (including area included in fuselage) ft	0.93
Leading edge of mean aerodynamic chord	Station 151.0
Root chord, ft	1.34
Tip chord, ft	0.29
Airfoil section, perpendicular to quarter-chord line	NACA 65009
Gap between tail and fuselage at 0° deflection, in.	1/16
Fuselage	
Fineness ratio	12.4
Ordinate at station x (x = 8.0 to x = 139.4) in.	$r = 8.5[1 - (x-102/102)^2]^{3/4}$

TABLE II.- ORDINATES OF WING AIRFOIL SECTION

Station, percent chord	Ordinate, percent chord
0	0
1	.298
2	.420
3	.512
5	.654
7.5	.790
10	.900
15	1.071
20	1.200
25	1.299
30	1.375
35	1.431
40	1.470
45	1.492
50	1.500
55	1.485
60	1.440
65	1.365
70	1.260
75	1.125
80	.960
85	.765
90	.540
95	.285
100	0

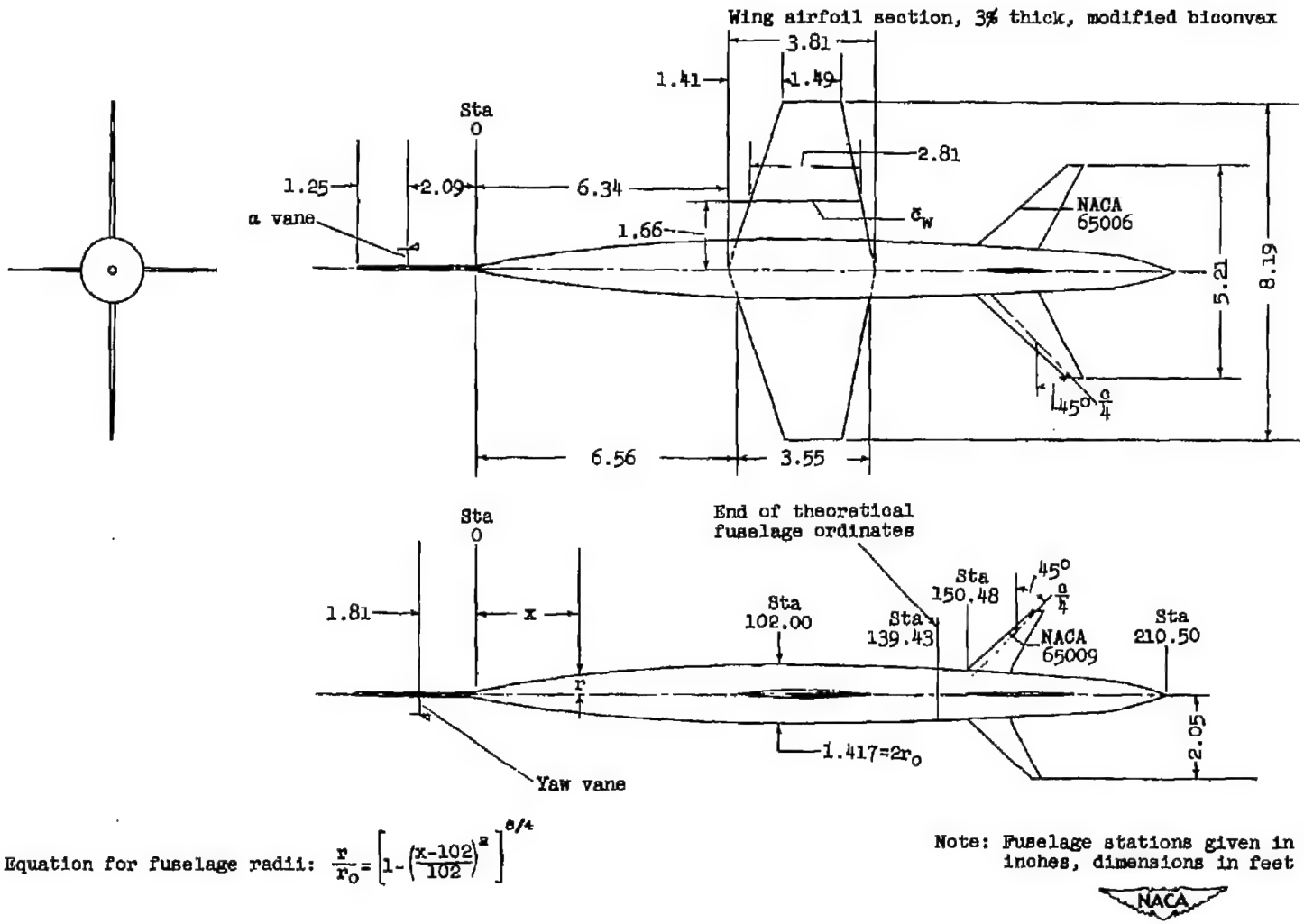

Figure 1.- Dimensional sketch of test model configuration.

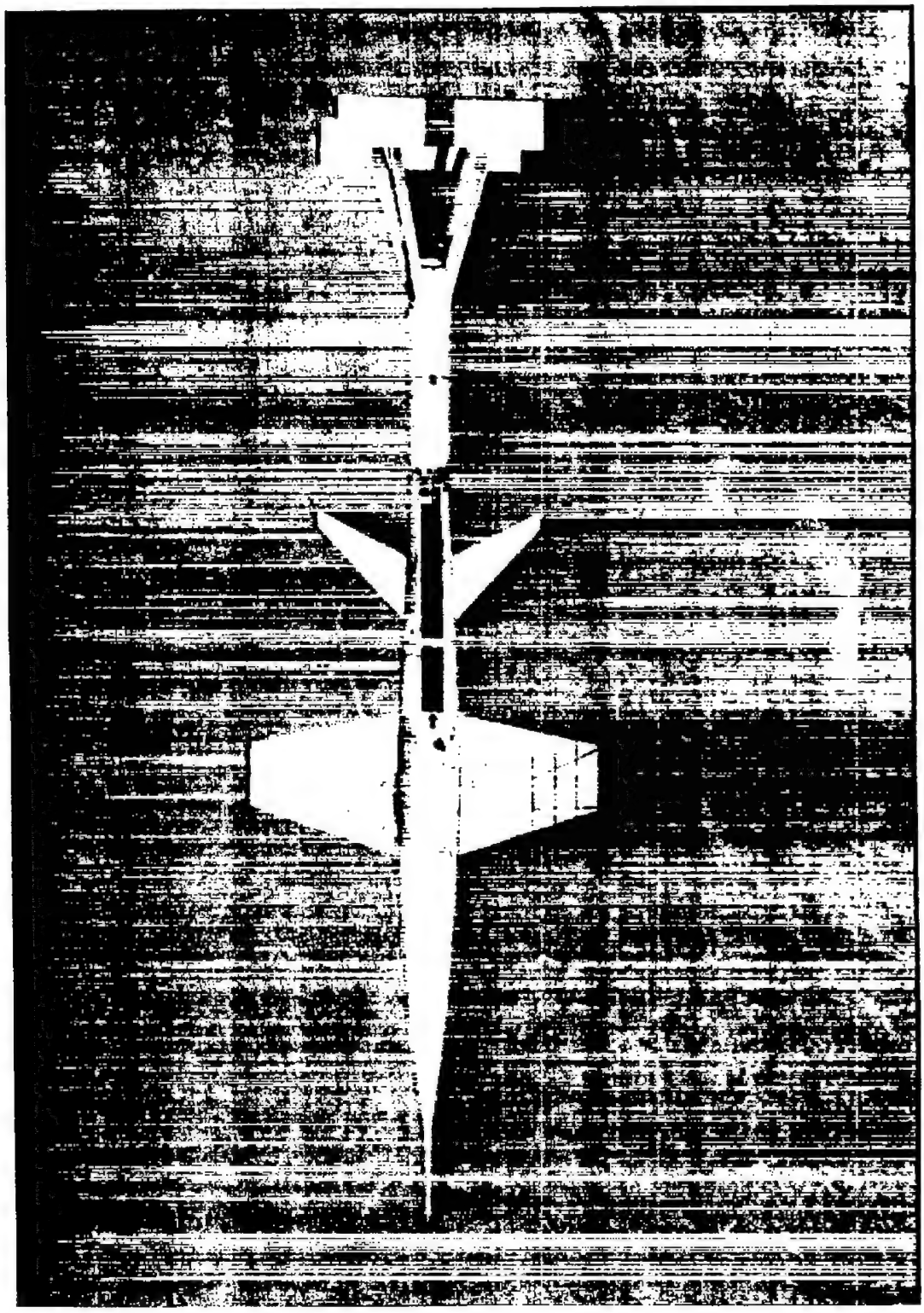

A-17772

Figure 2.- View of test model in free flight with booster attached.

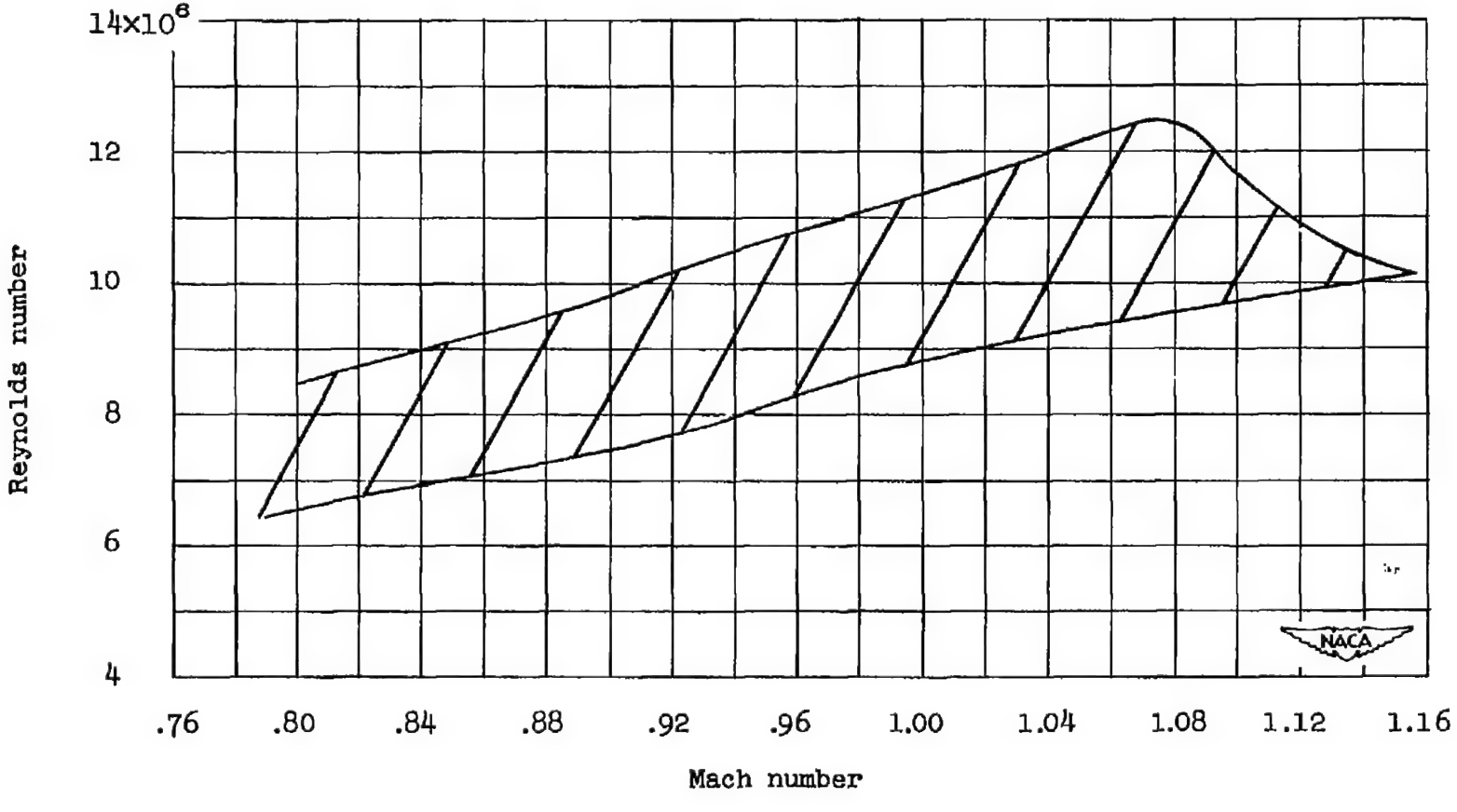

Figure 3.- Variation with Mach number of Reynolds number covered by test program.

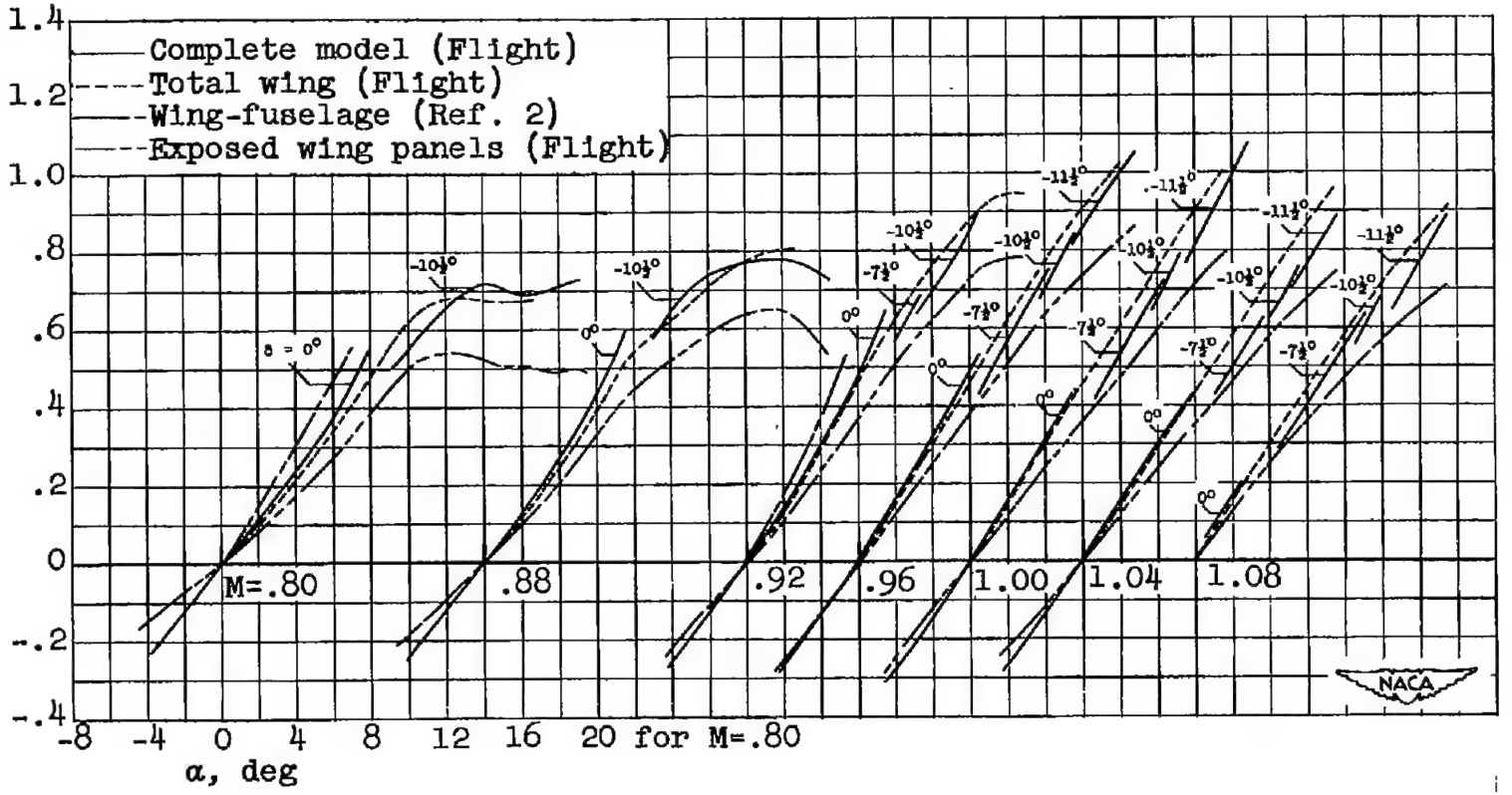

Figure 4.- Lift curves for various components of the test model.

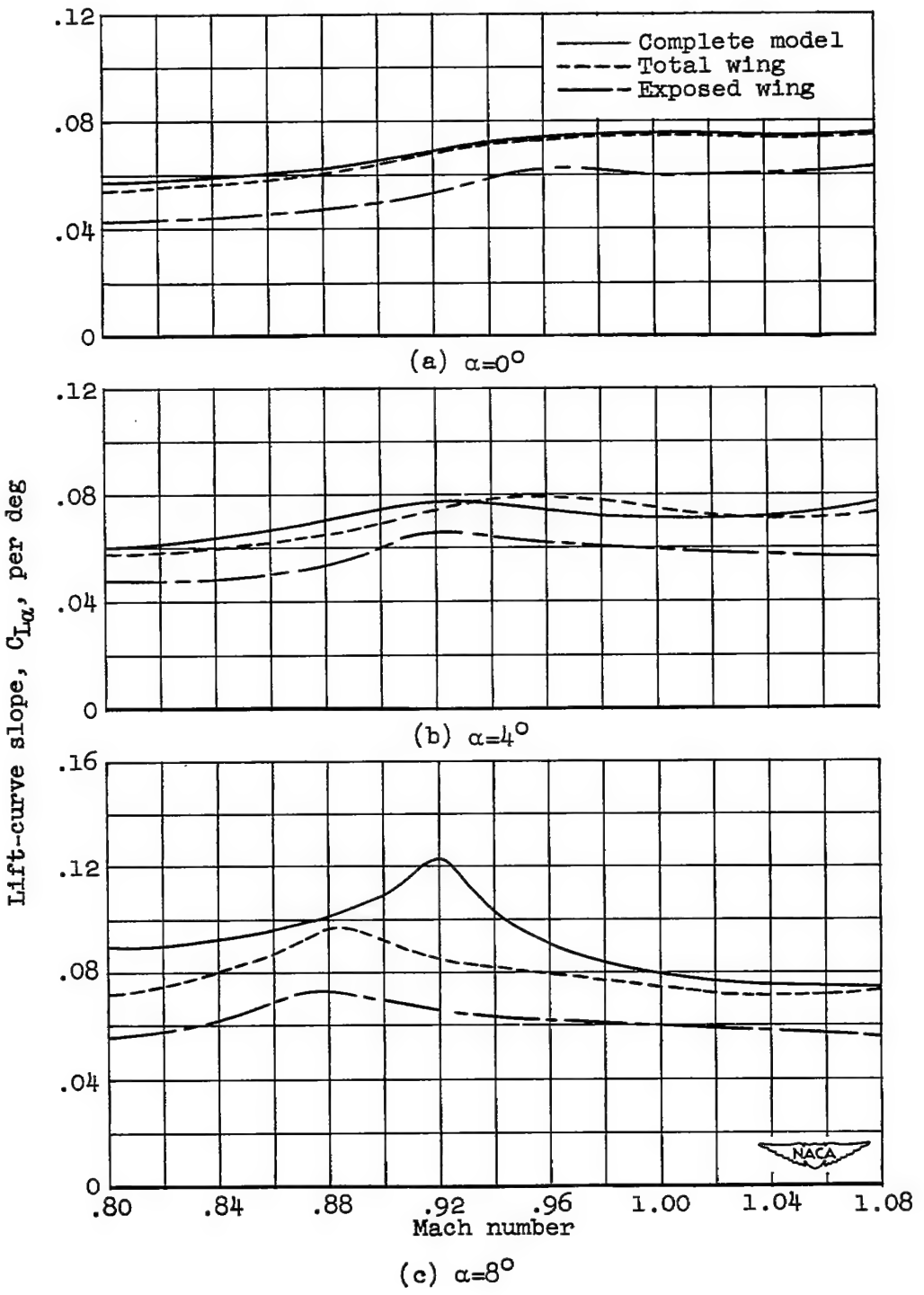

Figure 5.- Variation with Mach number of lift-curve slopes for various components of test model.

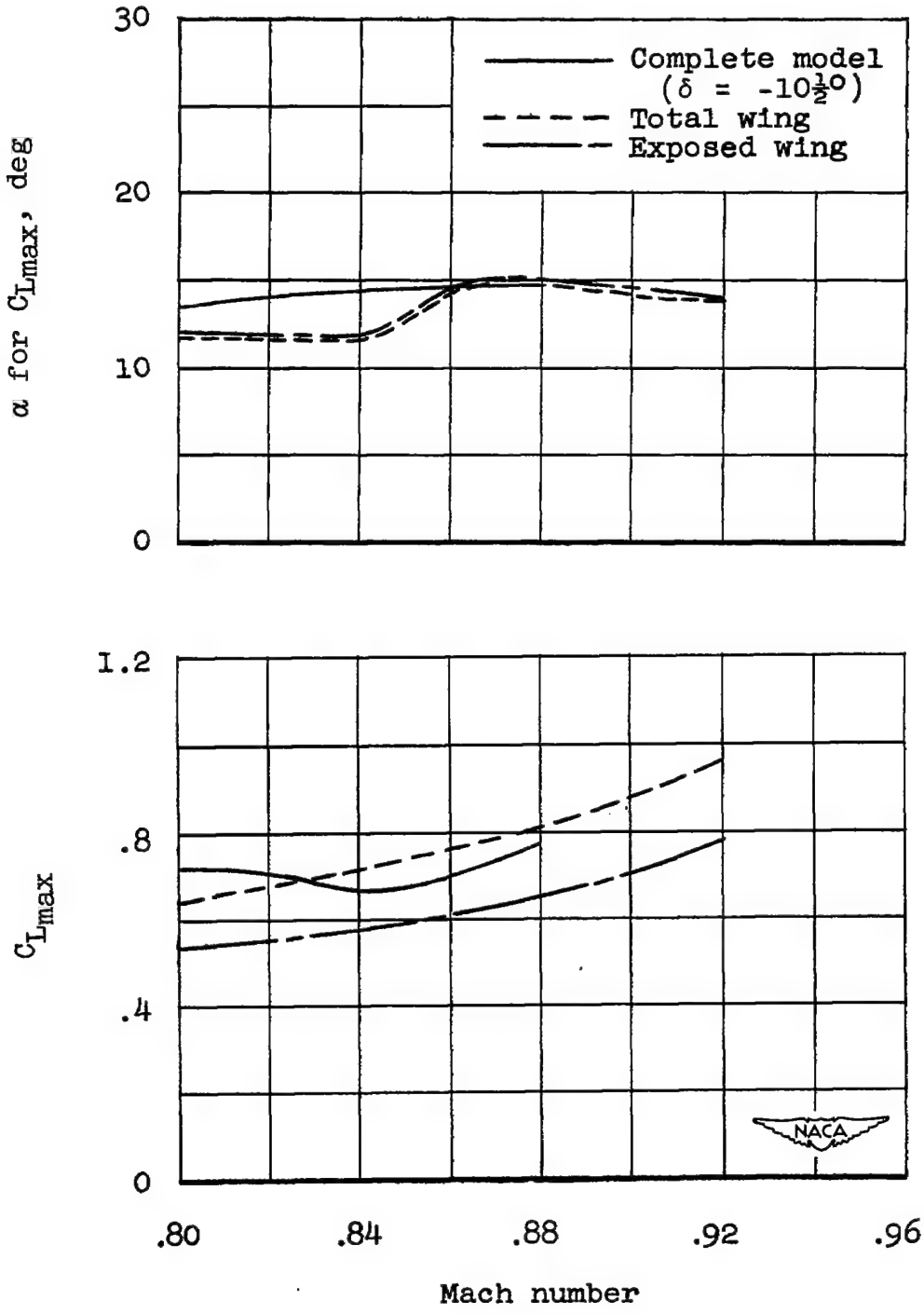

Figure 6.- Variation with Mach number of $C_{L_{max}}$ and α for $C_{L_{max}}$ for the test model.

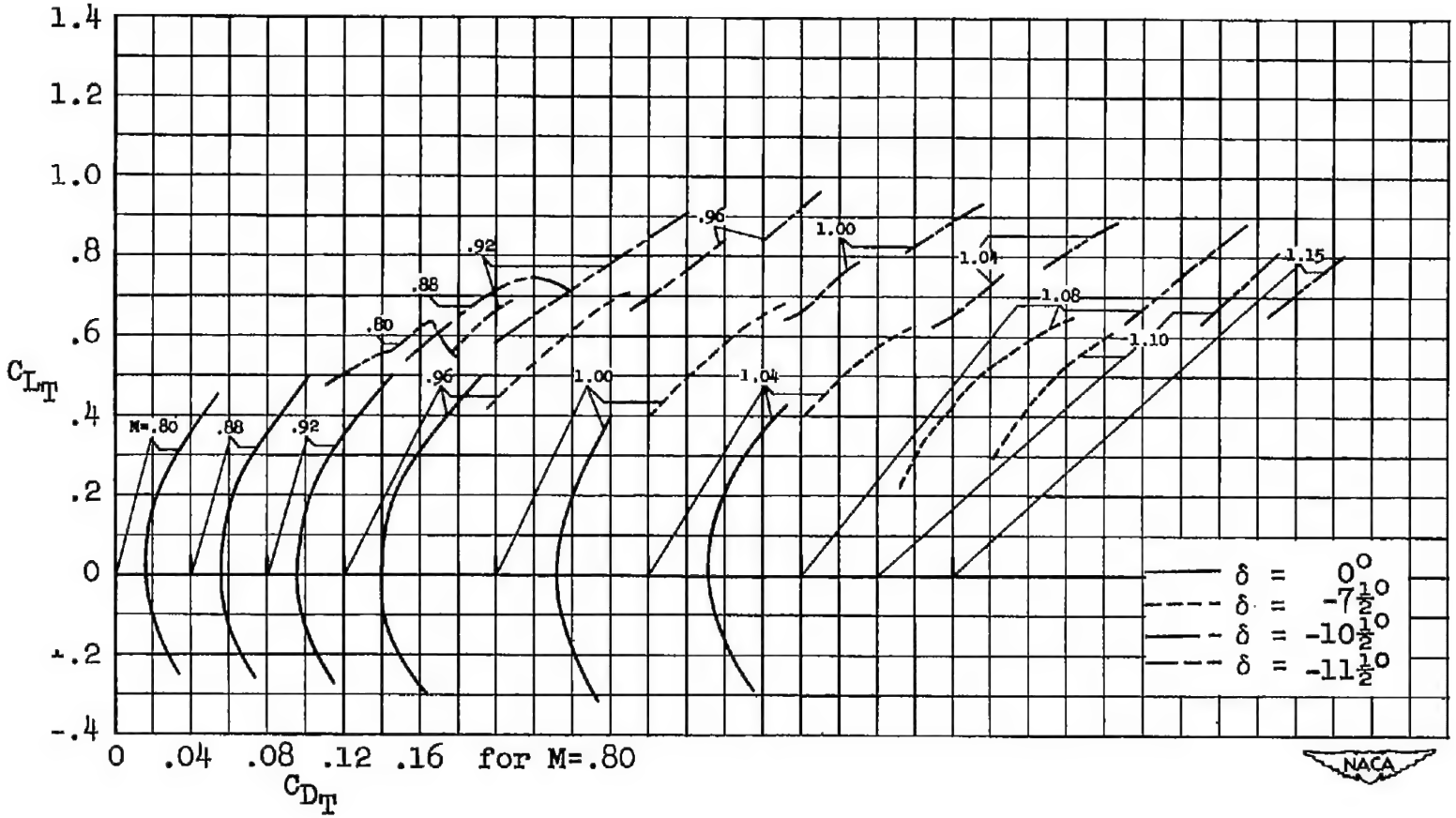

(a) Complete model.

Figure 7.- Variation of drag with lift for the complete model and for the wing at various Mach numbers.

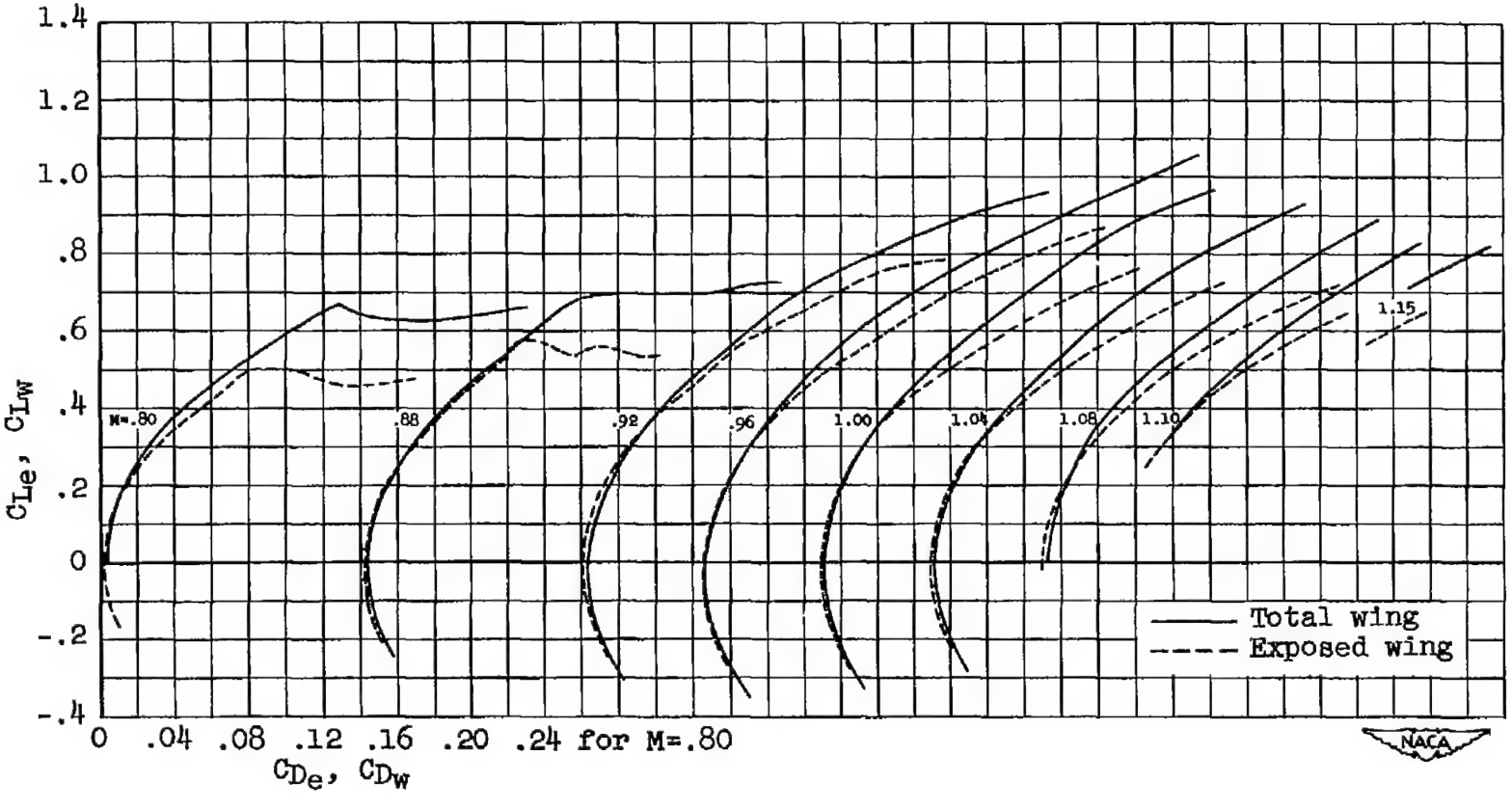

(b) Wing.

Figure 7.- Concluded.

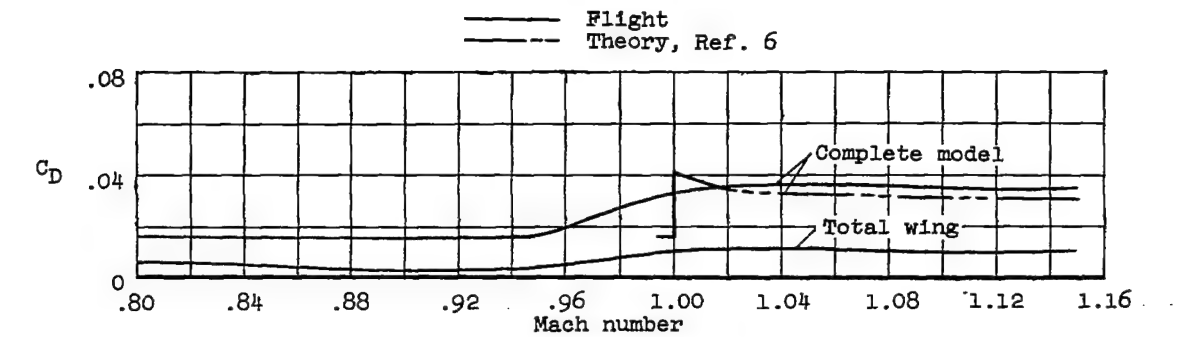

(a) Minimum drag.

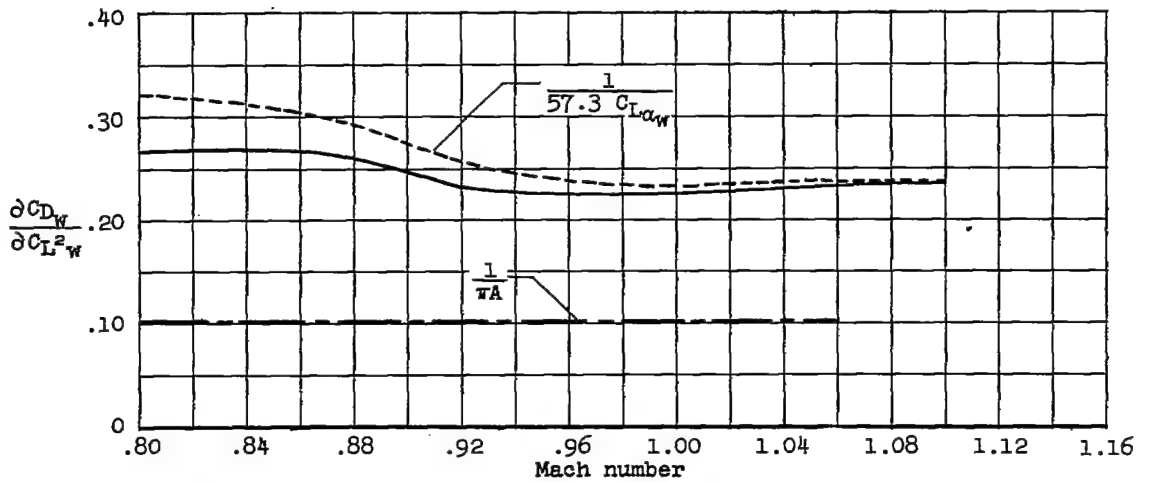

(b) Drag-rise with lift - wing.

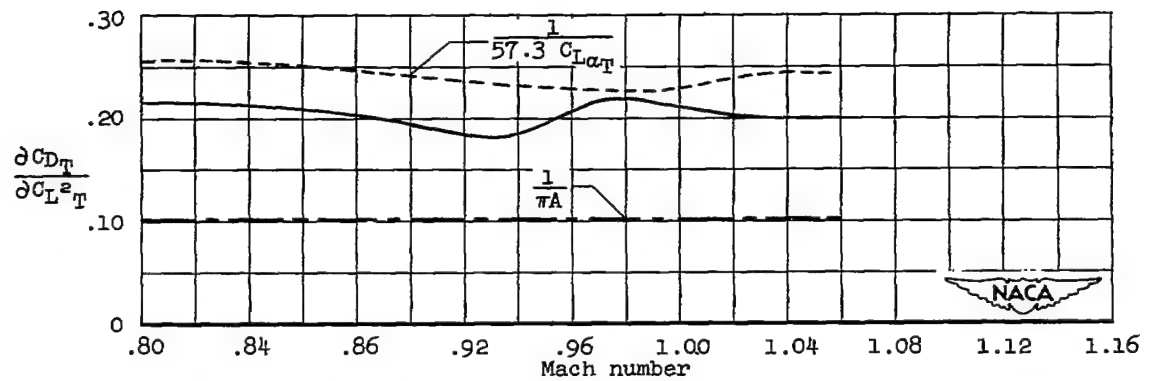

(c) Drag rise with lift - complete model.

Figure 8.- Variation with Mach number of drag-rise factor $\partial C_D/\partial C_L^2$ and of minimum drag coefficient for wing and for complete model.

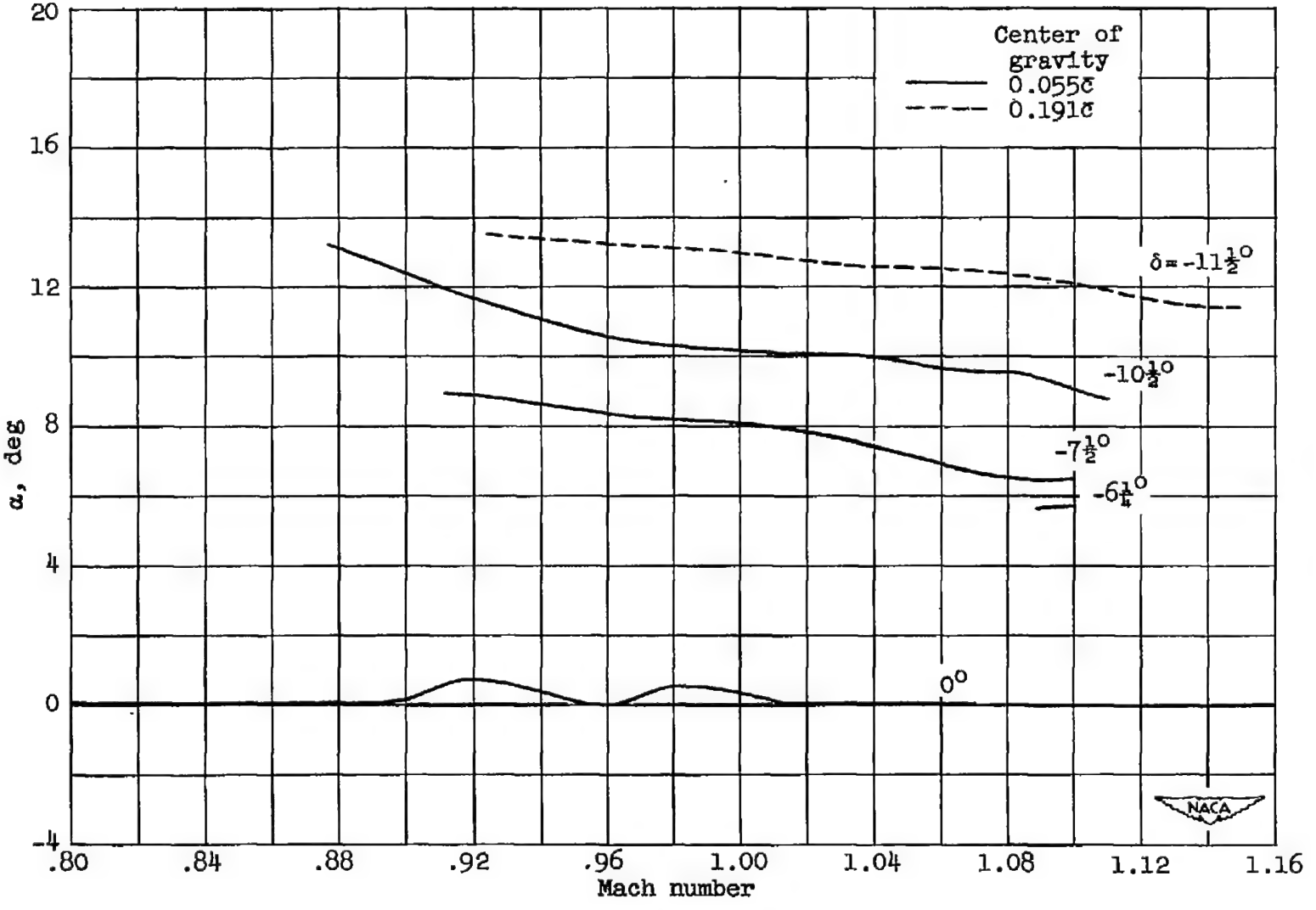

Figure 9.- Variation with Mach number of trim angle of attack for several horizontal tail settings.

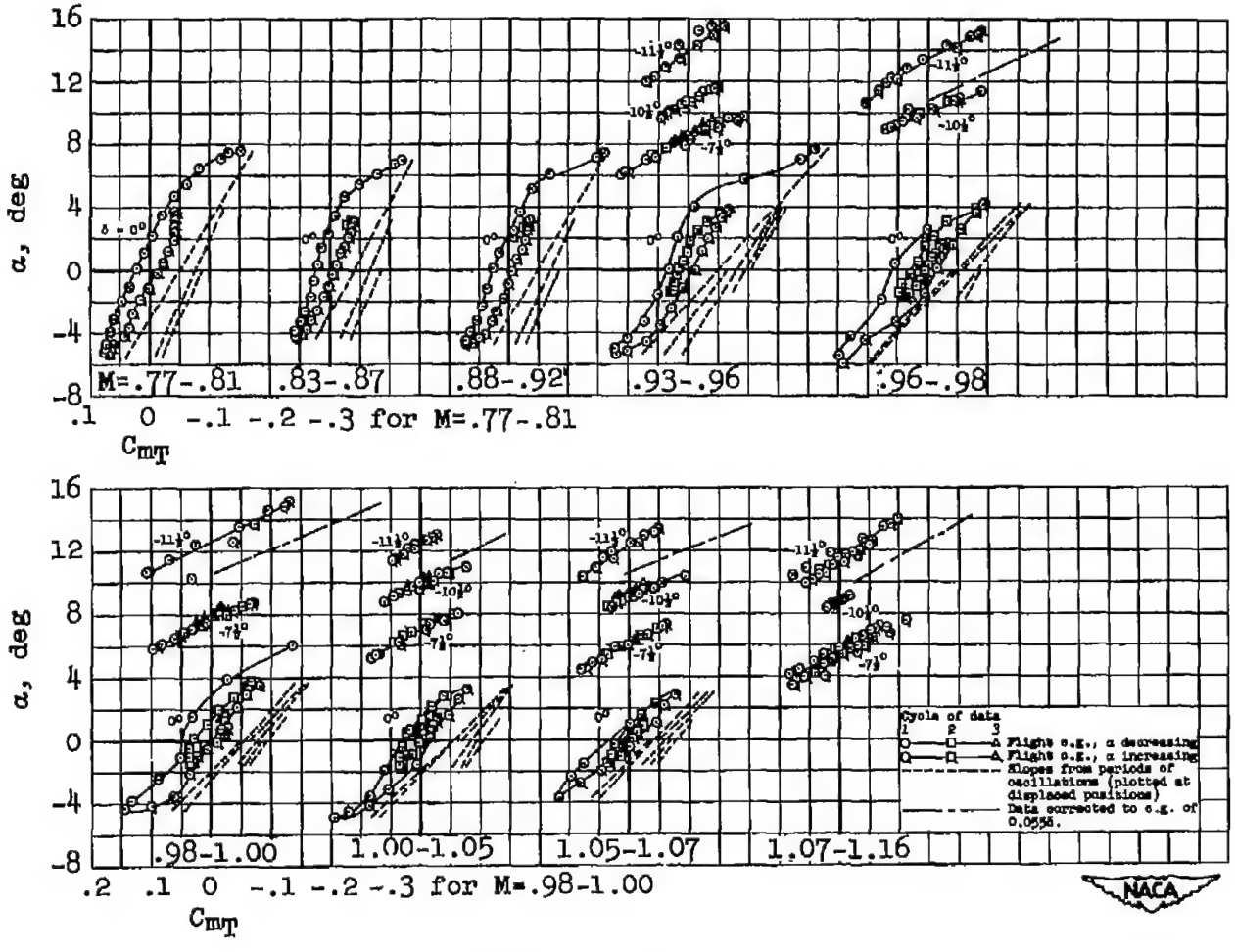

(a) Complete model.

Figure 10.- Variation with angle of attack of pitching-moment coefficients for total model and for exposed wing. Data for $\delta=0^\circ$, $-7\text{-}1/2^\circ$, $-10\text{-}1/2^\circ$ obtained with center of gravity at $0.055\bar{c}$; data for $\delta=-11\text{-}1/2^\circ$ obtained with center of gravity at $0.191\bar{c}$.

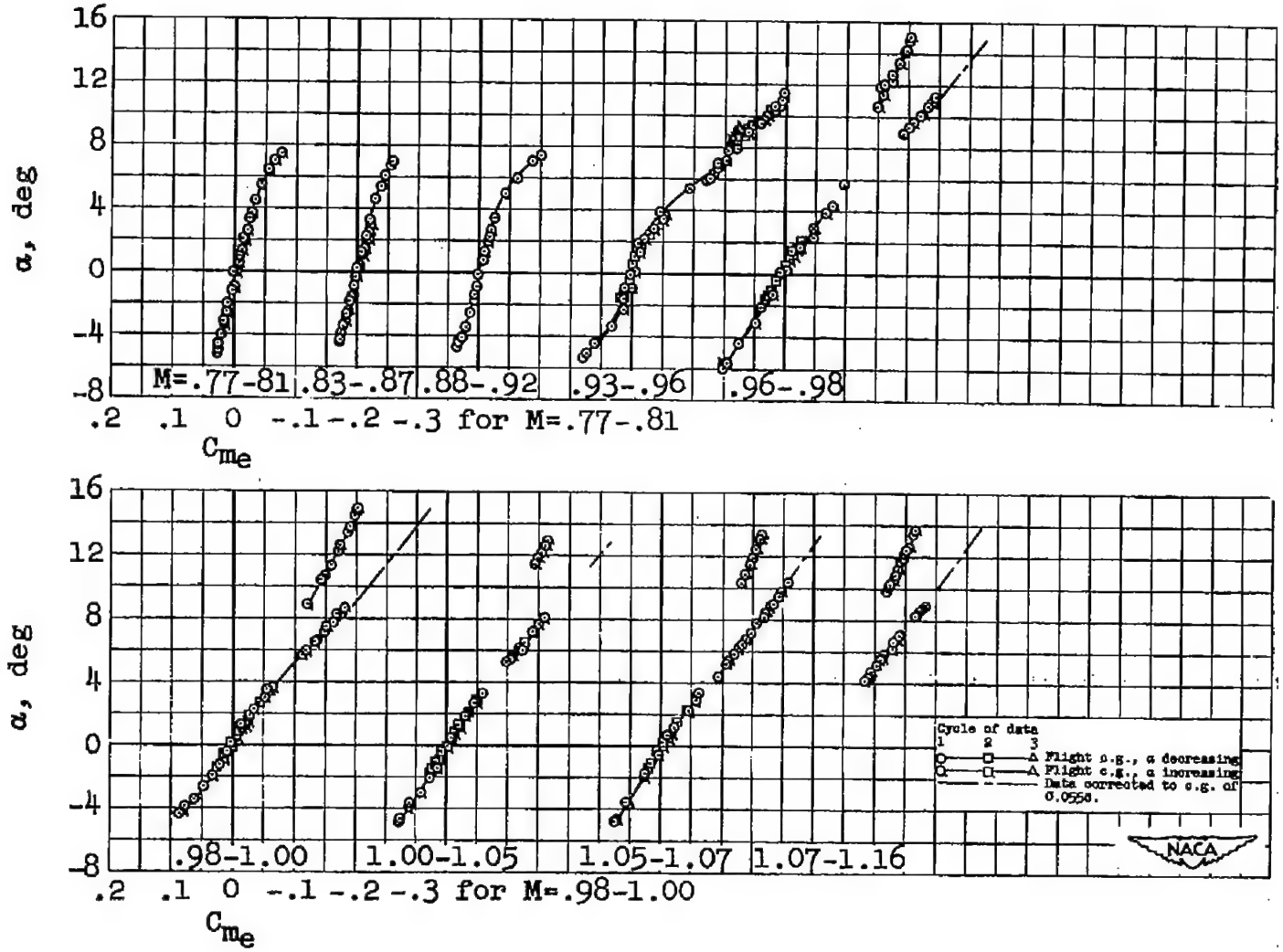

(b) Exposed wing.

Figure 10.- Concluded.

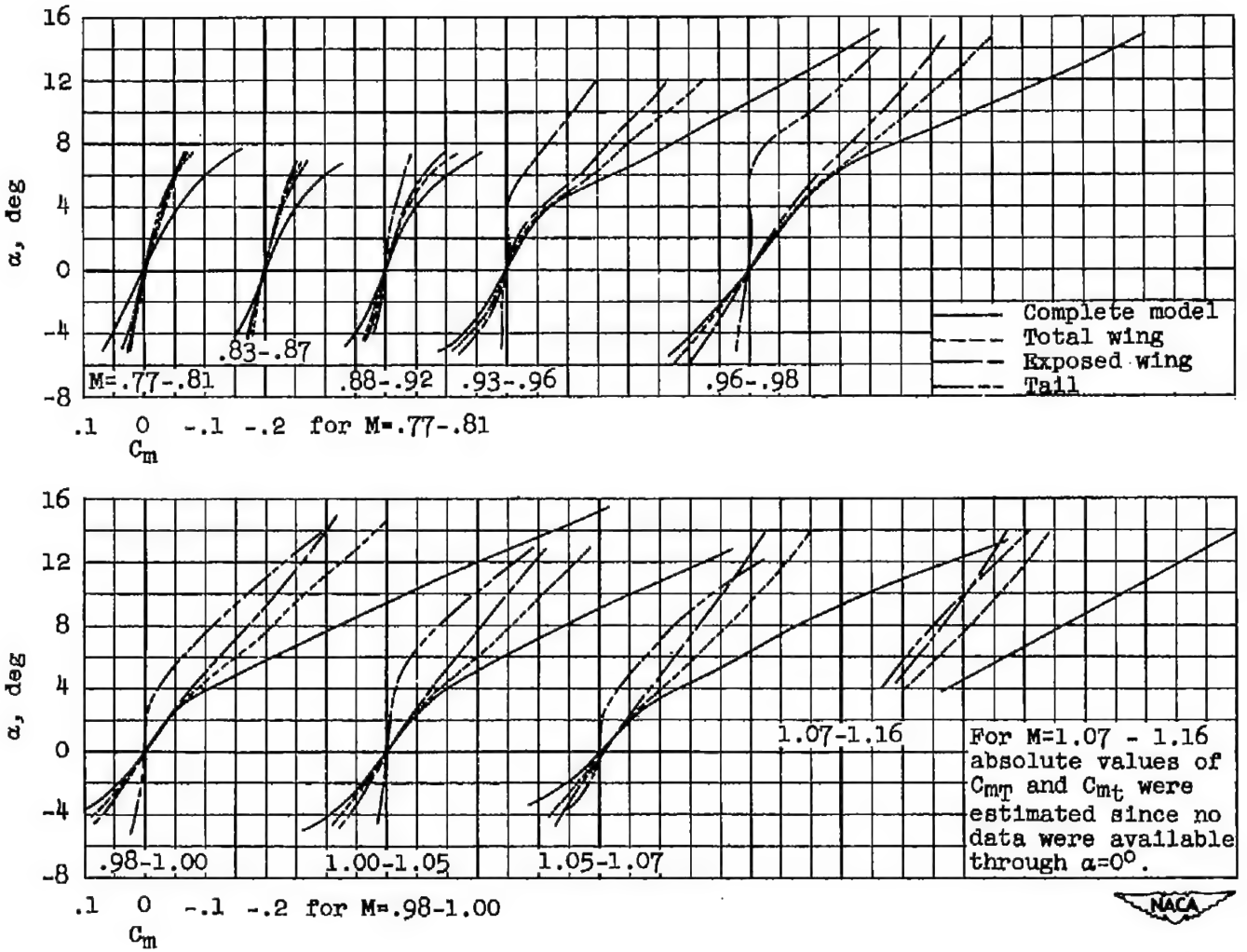

Figure 11.- Variation with angle of attack of pitching-moment coefficient of several components of model; center of gravity at 0.055$\bar{c}$, $\delta=0^{\circ}$.

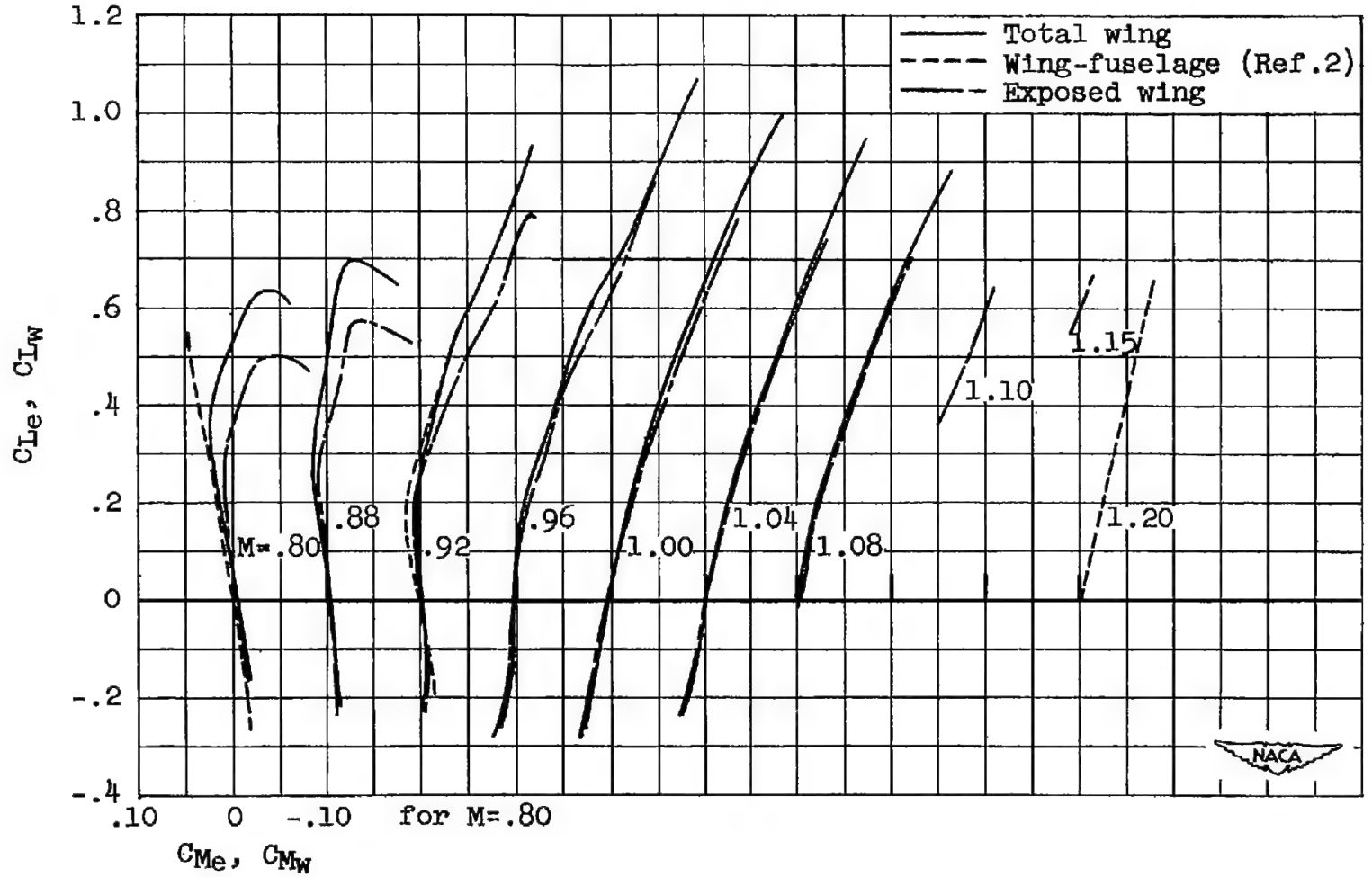

Figure 12.- Variation of pitching-moment coefficient with lift coefficient for wing of model; center of gravity at 0.25$\bar{c}$.

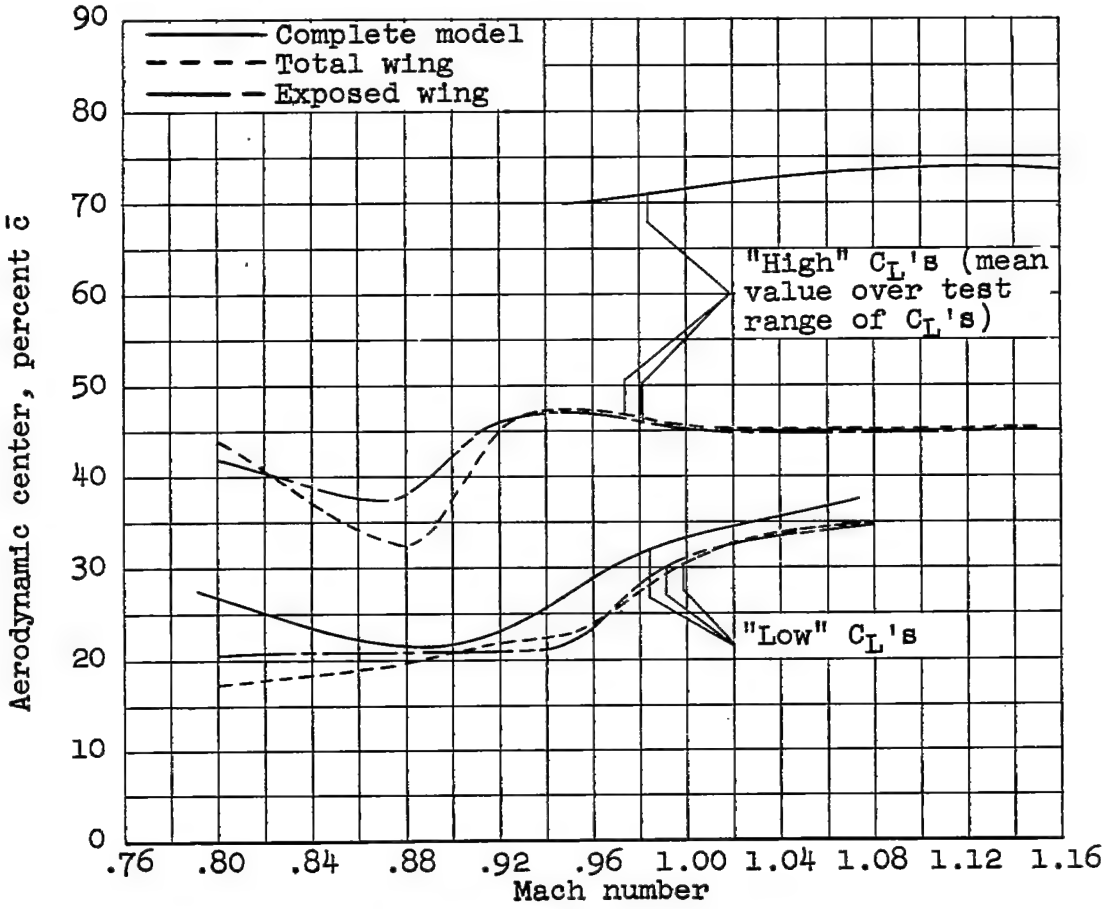

(a) Aerodynamic-center location.

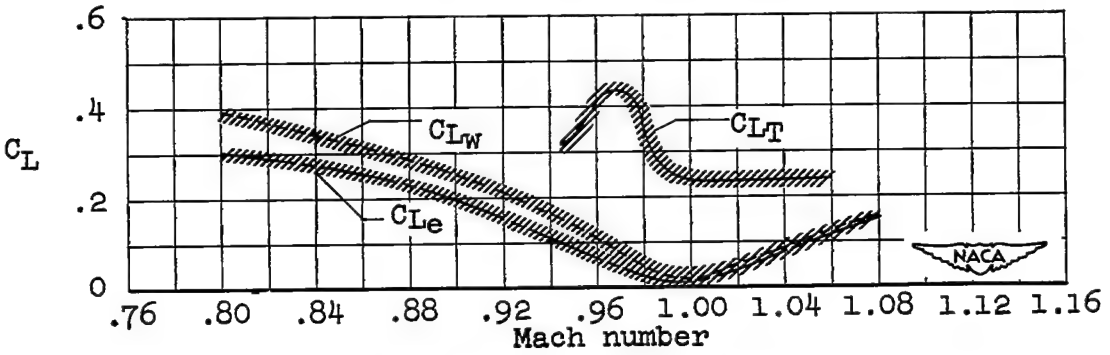

(b) Values of C_L at which stability changes from that for "low" C_L's to that for "high" C_L's.

Figure 13.- Variation with Mach number of aerodynamic-center location and of lift coefficient at which stability changes, for the wing and for the complete model.

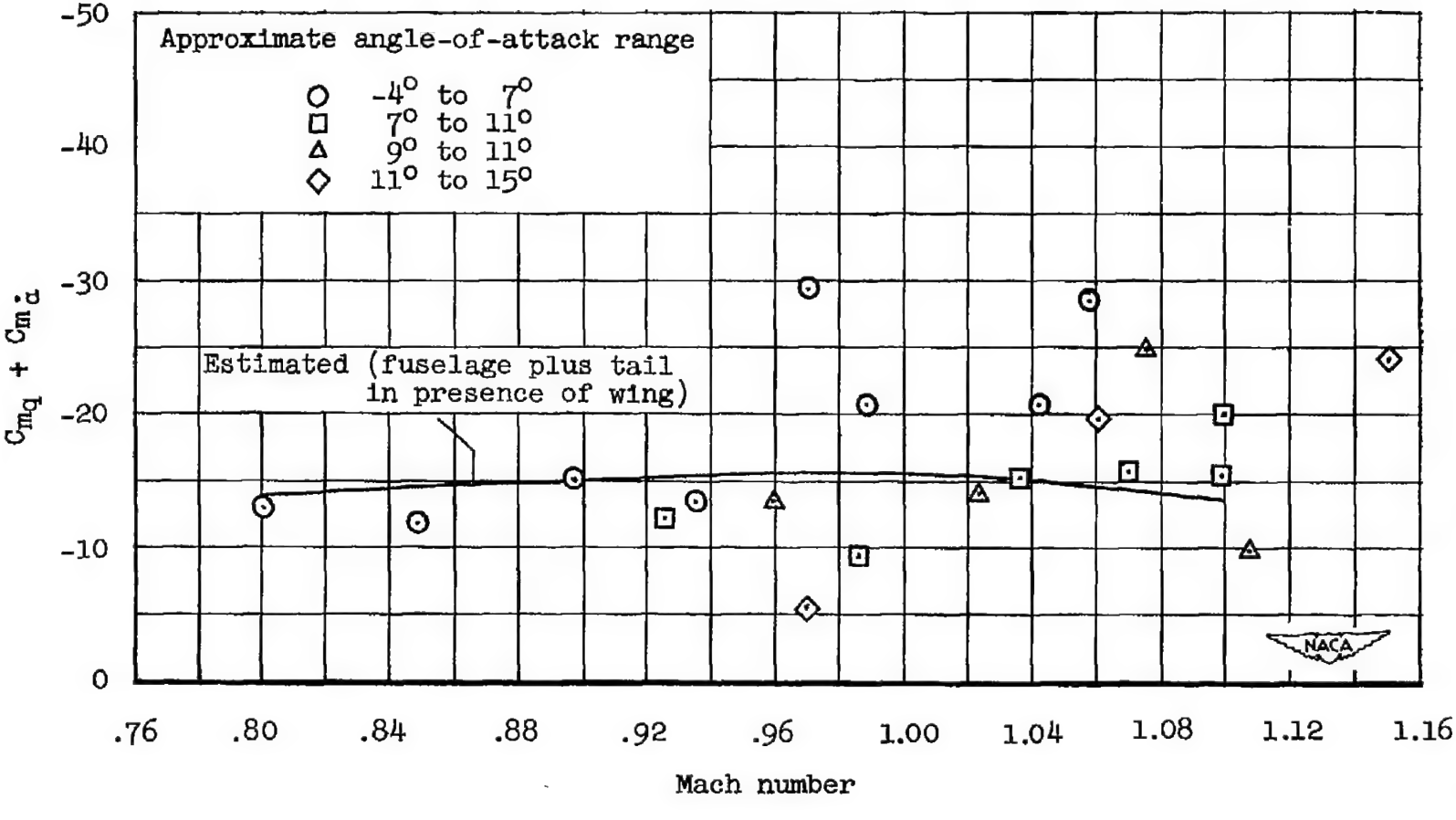

Figure 14.- Variation with Mach number of the damping-in-pitch parameter, $C_{m_q} + C_{m_{\dot{\alpha}}}$.

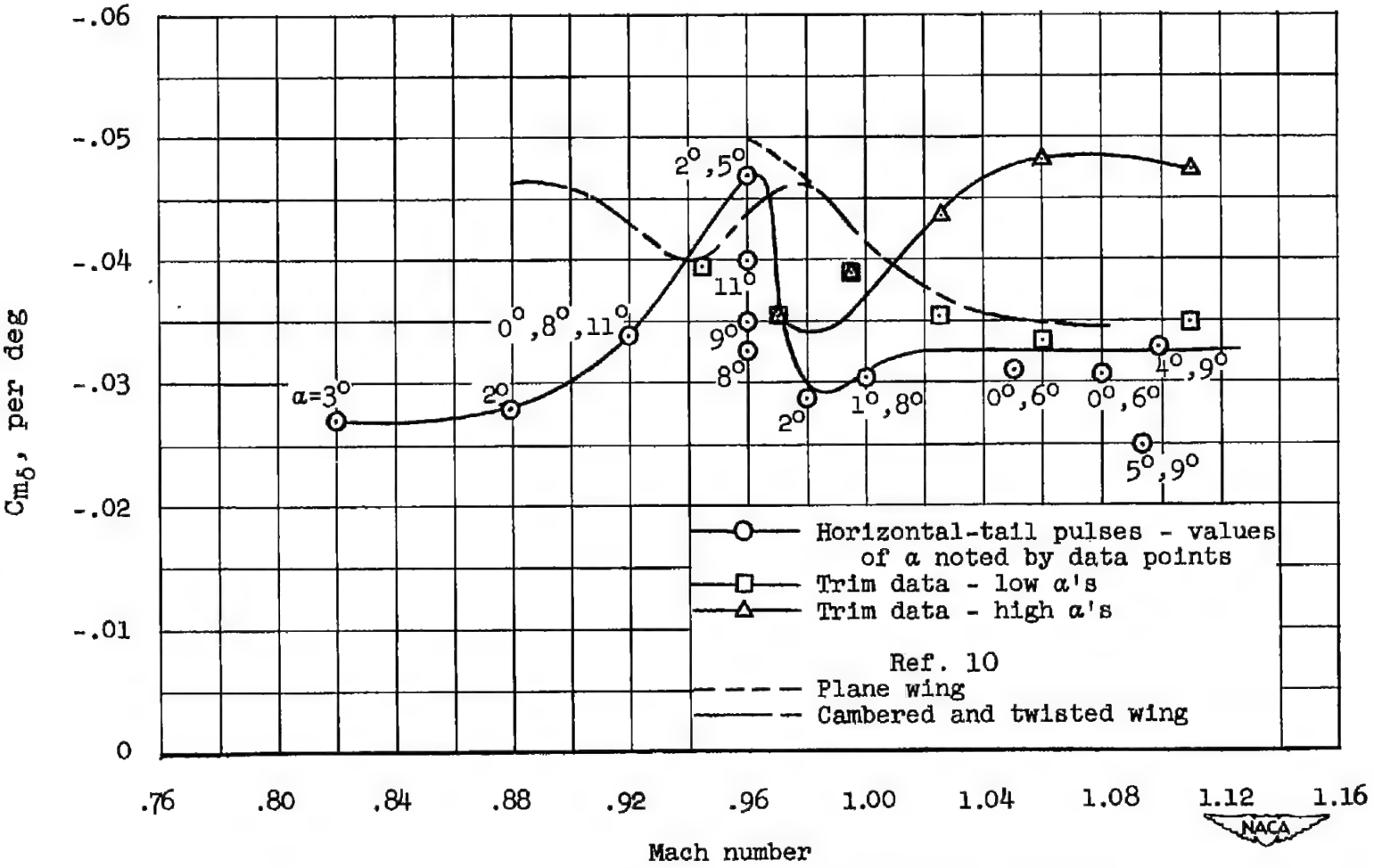

Figure 15.- Variation with Mach number of horizontal-tail-effectiveness parameter, C_{m_δ}; center of gravity at 0.055$\bar{c}$.

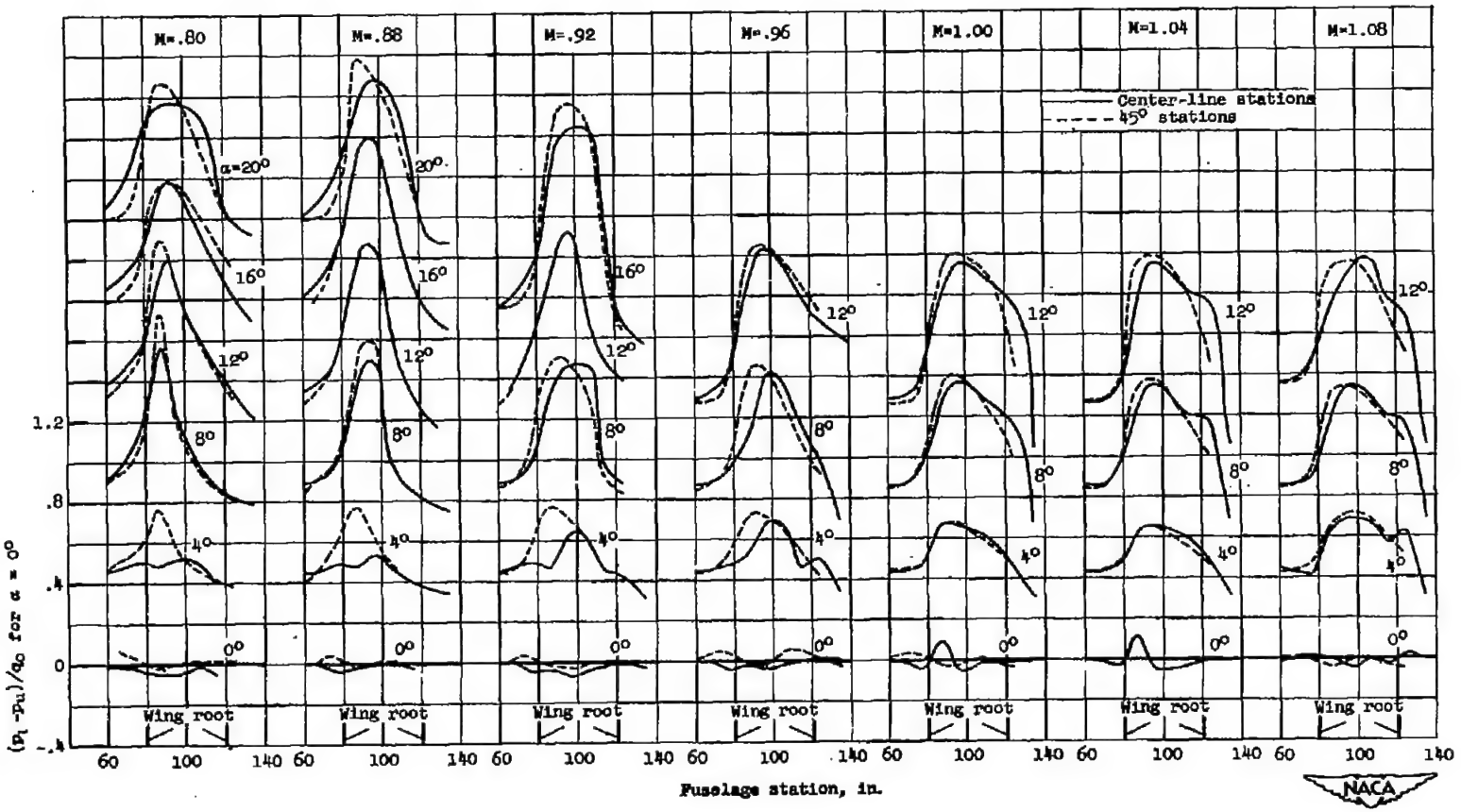

Figure 16.- Loading distribution over the fuselage in the vicinity of the wing.

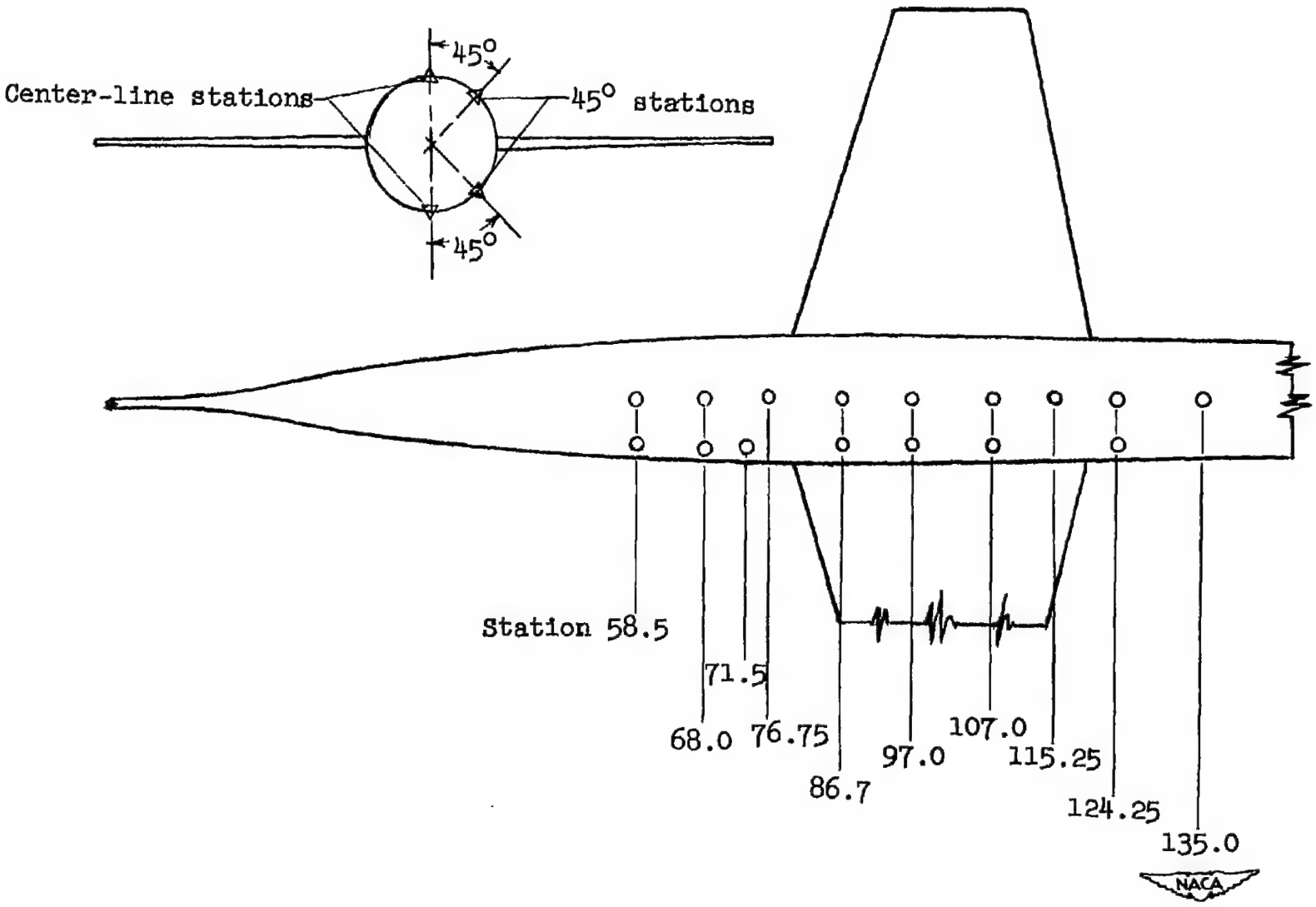

Figure 17.- Locations of pressure orifices on upper and lower surfaces of fuselage.

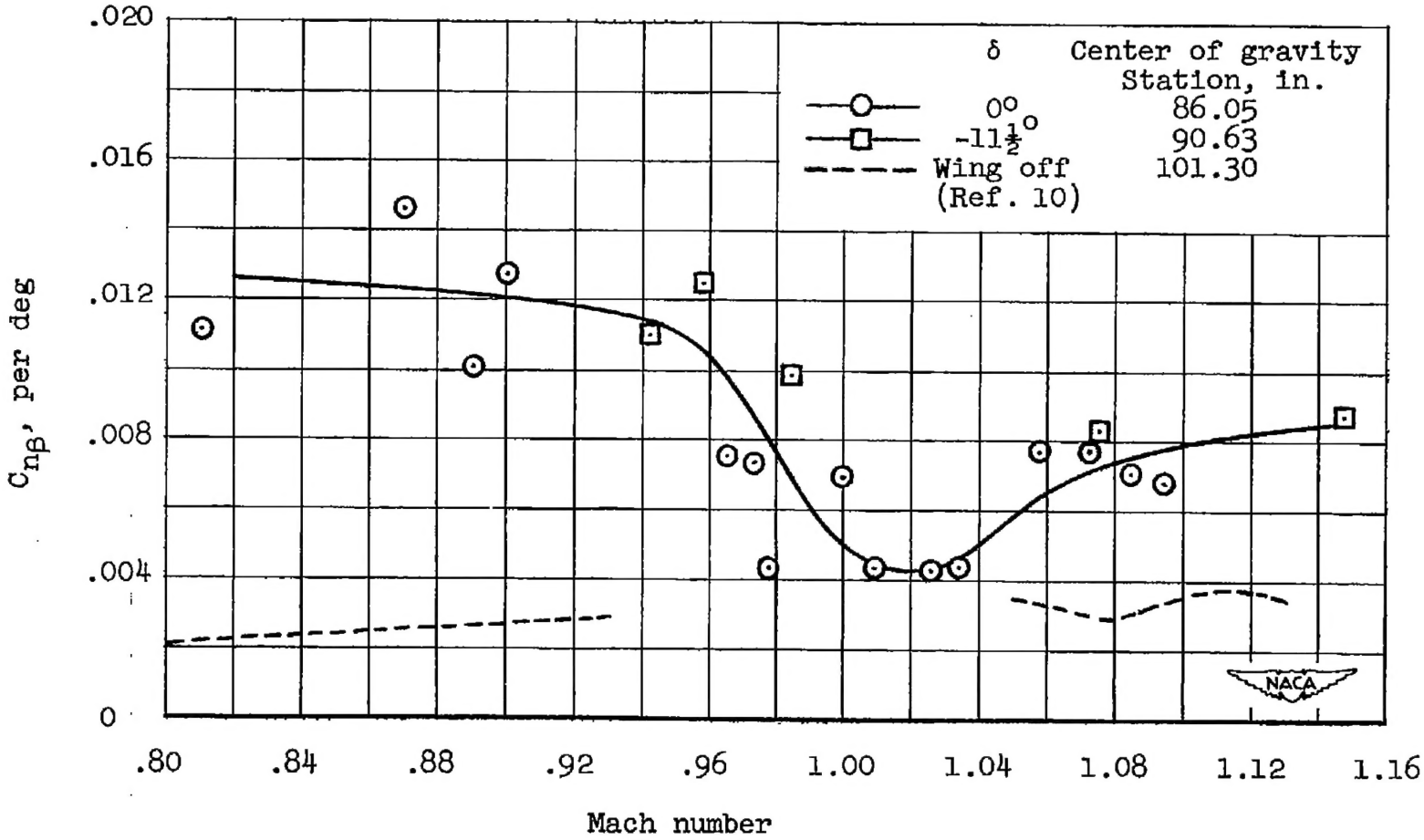

Figure 18.- Variation with Mach number of directional stability of test model.

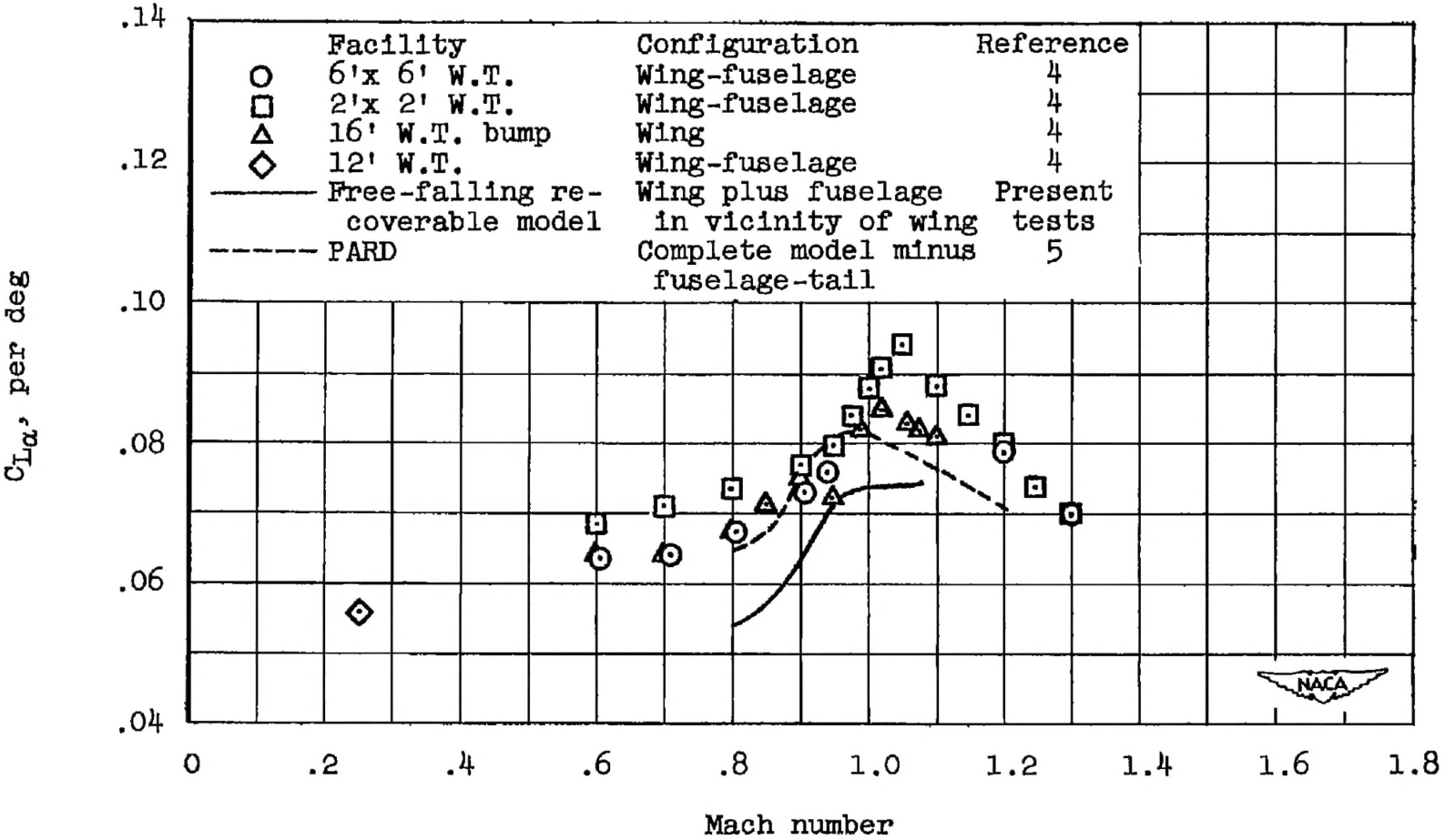

Figure 19.- Comparison of lift-curve slopes for total wing at zero lift as obtained from different tests.

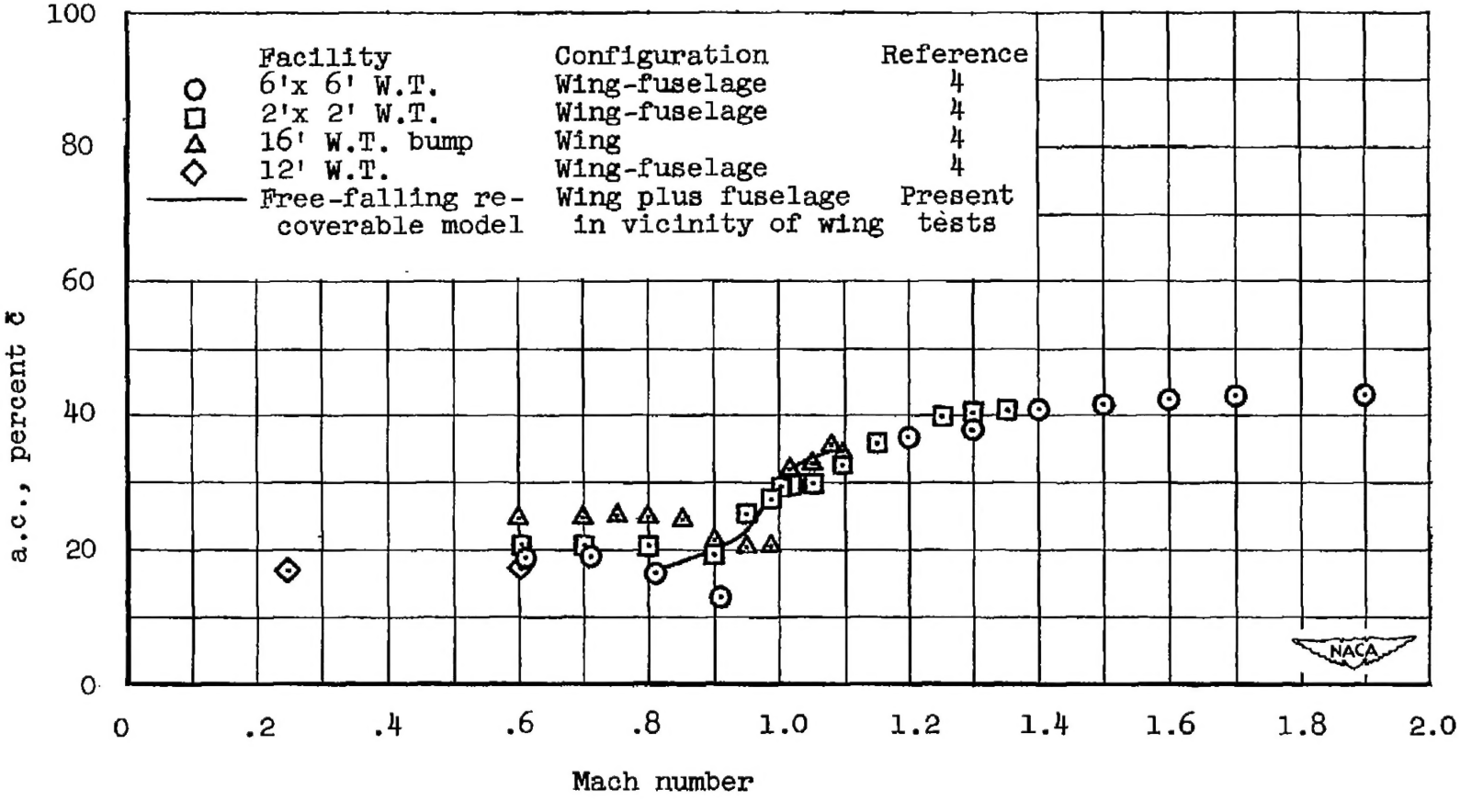

Figure 20.- Comparison of aerodynamic-center variations of total wing at low lift coefficients as obtained from different tests.

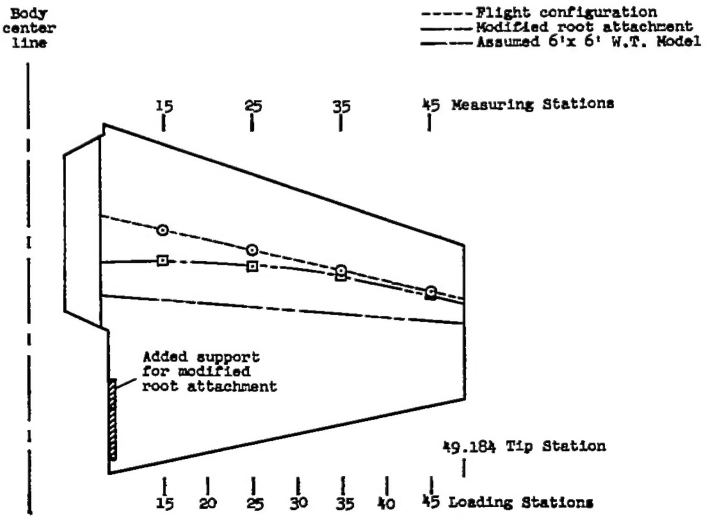

(a) Elastic axis location.

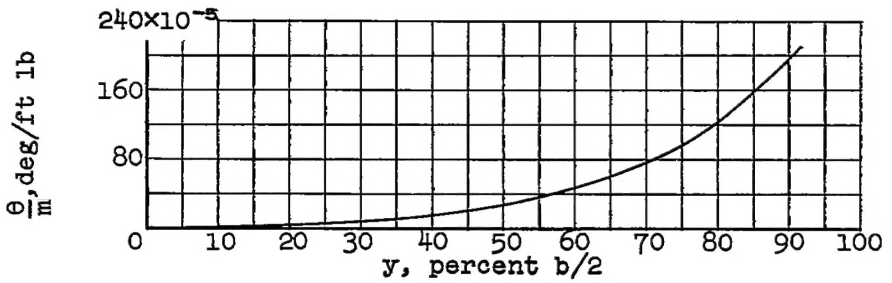

(b) Twisting deflection due to couple applied at wing tip.

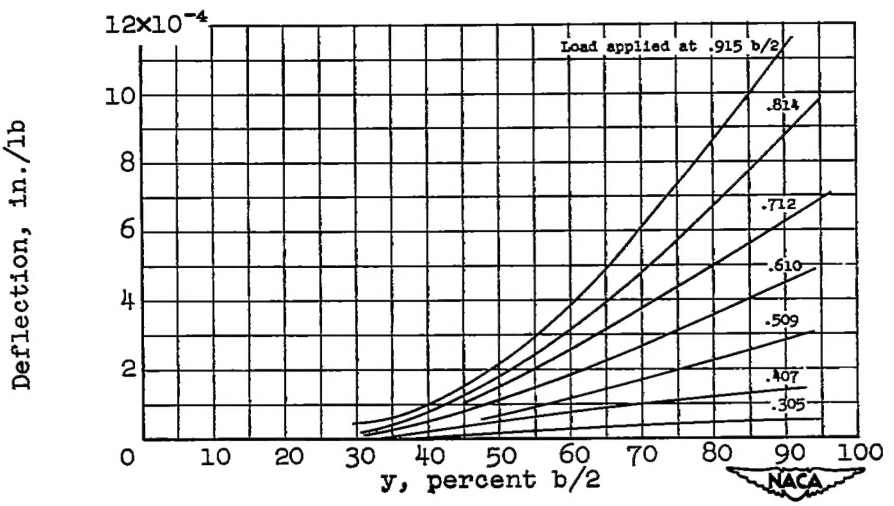

(c) Bending deflections due to unit load applied at elastic axis at various stations.

Figure 21.- Results of ground tests to determine elastic characteristics of test wing.

CONFIDENTIAL